

The *Hubble Space Telescope* Extragalactic Distance Scale Key Project. X. The Cepheid Distance to NGC 7331¹

Shaun M. G. Hughes,² Mingsheng Han,³ John Hoessel,⁴ Wendy L. Freedman,⁵ Robert C. Kennicutt, Jr.,⁶
 Jeremy R. Mould,⁷ Abi Saha,⁸ Peter B. Stetson,⁹ Barry F. Madore,¹⁰ Nancy A. Silbermann,¹¹
 Paul Harding,¹² Laura Ferrarese,¹³ Holland Ford,¹⁴ Brad K. Gibson,¹⁵ John A. Graham,¹⁶ Robert Hill,¹⁷
 John Huchra,¹⁸ Garth D. Illingworth,¹⁹ Randy Phelps,²⁰ Shoko Sakai²¹

Accepted for publication in the *Astrophysical Journal*, vol 501, 1998 July 1

¹Based on observations with the NASA/ESA *Hubble Space Telescope*, obtained at the Space Telescope Science Institute, which is operated by AURA, Inc. under NASA Contract No. NAS 5-26555.

²Royal Greenwich Observatory, Madingley Road, Cambridge CB3 0EZ, UK; hughes@ast.cam.ac.uk

³University of Wisconsin, Madison, Wisconsin 53706, USA; mhan@malachi.gsfc.nasa.gov

⁴University of Wisconsin, Madison, Wisconsin 53706, USA; hoessel@uwfpc.astro.wisc.edu

⁵The Observatories, Carnegie Institution of Washington, Pasadena, CA 91101; wendy@ociw.edu

⁶Steward Observatory, University of Arizona, Tucson, AZ 85721; robk@as.arizona.edu

⁷Mount Stromlo & Siding Spring Observatories, Australian National University, Canberra, Australia; jrm@merlin.anu.edu.au

⁸Space Telescope Science Institute, 3700 San Martin Drive, Baltimore, MD 21218; saha@stsci.edu

⁹Dominion Astrophysical Observatory, 5071 W. Saanich Rd., Victoria BC V8X 4M6; peter.stetson@hia.nrc.ca

¹⁰NASA/IPAC Extragalactic Database, Infrared Processing and Analysis Center, California Institute of Technology, Pasadena, CA 91125; barry@ipac.caltech.edu

¹¹Infrared Processing and Analysis Center, Jet Propulsion Laboratory, California Institute of Technology, Pasadena, CA 91125; nancys@ipac.caltech.edu

¹²Steward Observatory, University of Arizona, Tucson, AZ 85721; harding@as.arizona.edu

¹³Palomar Observatory, California Institute of Technology, Pasadena, CA 91125; lff@astro.caltech.edu

¹⁴Dept of Physics & Astronomy, Bloomberg 501, Johns Hopkins Univ., 3400 N. Charles St., Baltimore, MD 21218; ford@stsci.edu

¹⁵Mount Stromlo & Siding Spring Observatories, Australian National University, Canberra, Australia; gibson@mso.anu.edu.au

¹⁶Department of Terrestrial Magnetism, Carnegie Institution of Washington, 5241 Broad Branch Rd. N.W., Washington D.C. 20015; graham@jag.ciw.edu

¹⁷Laboratory for Astronomy & Solar Physics, NASA Goddard Space Flight Center, Greenbelt, MD 20771; hill@esa.nascom.nasa.gov

¹⁸Harvard-Smithsonian Center for Astrophysics, 60 Garden Street, Cambridge, MA 02138; huchra@cfa.harvard.edu

¹⁹Lick Observatory, University of California, Santa Cruz, CA 95064; gdi@ucolick.org

²⁰The Observatories, Carnegie Institution of Washington, Pasadena, CA 91101; phelps@ociw.edu

²¹Infrared Processing and Analysis Center, Jet Propulsion Laboratory, California Institute of Technology, Pasadena, CA 91125; shoko@ipac.caltech.edu

ABSTRACT

The distance to NGC 7331 has been derived from Cepheid variables observed with HST/WFPC2, as part of the Extragalactic Distance Scale Key Project. Multi-epoch exposures in F555W ($\sim V$) and F814W ($\sim I$), with photometry derived independently from DoPHOT and DAOPHOT/ALLFRAME programs, were used to detect a total of 13 reliable Cepheids, with periods between 11 and 42 days. The relative distance moduli between NGC 7331 and the LMC, derived from the V and I magnitudes, imply an extinction to NGC 7331 of $A_V = 0.47 \pm 0.15$ mag, and an extinction-corrected distance modulus to NGC 7331 of $30.89 \pm 0.14(\text{random})$ mag, equivalent to a distance of $15.1^{+1.0}_{-0.9}$ Mpc. There are additional systematic uncertainties in the distance modulus of ± 0.12 mag due to the calibration of the Cepheid Period-Luminosity relation, and a systematic offset of $+0.05 \pm 0.04$ mag if we applied the metallicity correction inferred from the M101 results of Kennicutt et al 1998.

Subject headings: Cepheids — galaxies: distances and redshifts — galaxies: individual (NGC 7331) — stars: early type — stars: luminosity function — techniques: photometric

1. Introduction

The *Hubble Space Telescope* (HST) Extragalactic Distance Scale Key Project aims to obtain Cepheid distances to 18 galaxies within 20 Mpc, to use these to calibrate secondary distance estimators, and thereby measure H_0 to an external accuracy of 10% (Kennicutt, Freedman & Mould 1995). NGC 7331 (Figure 1) was chosen primarily as a calibrator for the luminosity-line width relation (also known as the Tully-Fisher relation). It lies in the constellation of Pegasus, at position $\alpha = 22^{\text{h}}37^{\text{m}}05^{\text{s}}.2$, $\delta = +34^{\circ}25'10''$ (J2000), and has a Galactocentric velocity of +1035 km/s (de Vaucouleurs et al. 1991; hereinafter RC3).

NGC 7331 has an early type spiral classification of Sb(rs)I-II in the Revised Shapley-Ames scheme by Sandage & Tammann (1981), a Hubble type T = 3 in RC3, and an inclination of $\sim 75^\circ$ (estimates vary from 71° by Huchtmeier & Richter 1989 to $75 \pm 5^\circ$ by Marcelin et al. 1994 and $74.8 \pm 2.0^\circ$ by Begeman 1987). The H II rotation curve for NGC 7331 is very regular, and peaks at ~ 250 km/s (Rubin et al. 1965), and the H I (21 cm) linewidth (W_{20}) has been measured as 531 ± 10 km/s (Fisher & Tully 1981) and 536 km/s (from Begeman 1987). The properties of being a regular spiral of moderately large inclination make NGC 7331 an ideal calibrator for the Tully-Fisher relation.

We present here the distance to NGC 7331, using observations obtained with the post-repair mission Wide Field and Planetary Camera (WFPC2) on HST with the F555W and F814W filters (see Holtzman et al. 1995a, and the current version of the WFPC2 Instrument Handbook from STScI, for details of the performance of WFPC2). Our methodology follows that used in previous papers in this series: e. g. M81 (Freedman et al. 1994a), M100 (Freedman et al. 1994b and Ferrarese et al. 1996), M101 (Kelson et al. 1996), NGC 925 (Silbermann et al. 1996), NGC 2090 (Phelps et al. 1998), NGC 3351 (Graham et al. 1997), and NGC 3621 (Rawson et al. 1997). Photometry for all epochs was obtained with programs designed for crowded fields (§ 2). The resultant lightcurves were then searched to identify and measure periods and luminosities of 13 Cepheid variables (§ 3), applying the calibrations described in Ferrarese et al. (1996) and Hill et al. (1998). Period-luminosity relations were fitted to these Cepheids, relative to the Large Magellanic Cloud (LMC), to derive extinction-corrected distance moduli for each photometry set (§ 4). Implications

for the properties of NGC 7331, and previous calibrations of the Tully-Fisher (TF) relation (§ 5) are briefly discussed. Preliminary results of this work were described in Hughes, Han & Hoessel (1996).

2. Photometry

The WFPC2 field lies 3.5 arcmin north of the galaxy’s nucleus, along the major axis (Figures 1 and 2). Variable stars were detected from 15 epochs of F555W cosmic ray-split exposures, and their colors were measured from 4 epochs of F814W exposures, over the interval of 1994 June 18 to 1995 August 17, as listed in Table 1. Each cosmic ray-split exposure pair consisted of a 1600 sec and a 1200 sec exposure (a safing event part way through the series meant that three F555W and one F814W epochs had to be postponed, and resulted in missed 1600 sec exposures for F555W at epoch 7 and F814W at epoch 8). In all cases the gain was $7 \text{ e}^-/\text{DN}$, with a readout noise of 7 e^- . All of these epochs were taken after the decrease in the WFPC2 operating temperature (which occurred on 1994 April 23). Although there appears to be a charge transfer efficiency effect in the WFPC2 CCDs, this may be significant only in exposures with a low background, and seems to be negligible for backgrounds brighter than 70e^- (Rawson et al. 1997). As our NGC 7331 frames all have backgrounds brighter than 70e^- , they should not have been affected. Two short exposures of 260 sec in F555W and F814W were also made at epoch 13, but have not been used as they were intended for calibration backup via ground-based observations in case there were any problems with the photometric calibrations.

The science frames were processed through the standard STScI pipeline (Holtzman et al. 1995a). The photometric distortions introduced by the WFPC2 corrective optics were rectified by multiplying each image by a pixel area correction map. These differ slightly from those used by Holtzman et al. (1995b) in that the normalization is relative to the median pixel, rather than the largest.

Various pixels were systematically ignored by the photometry programs: those which are off the WFPC2 pyramid surface; or vignetted by the pyramid edge; or given a non-zero value in the bad pixel maps.

The photometry was derived using two independent programs, in order to identify and trap any possible mistakes in the reduction process by comparing their final results. The first program is based on DoPHOT (Schechter, Mateo & Saha 1993; Saha et al. 1994; Saha et al. 1996), and the second is DAOPHOT/ALLFRAME (Stetson 1994), used in a similar way as described in detail for M100 by Ferrarese et al. (1996) and Hill et al. (1998), adopting the long exposure calibration (see Appendix).

2.1. DoPHOT

DoPHOT measures magnitudes by fitting a purely analytic model point-spread function (PSF) to objects detected above a user-specified threshold. For DoPHOT, we followed the methodology described in Saha et al. (1996; sections 2 and 3),²² which we will only briefly describe here. Each cosmic ray-split pair of observations was first combined using a sigma detection algorithm which takes into account the problems of undersampling (see Saha et al. 1996 for a full description), to produce single frames per epoch mostly

²²With the exception that here we have corrected for the photometric distortions of the corrective optics by the multiplication of the pixel area map.

free of cosmic rays. The cosmic ray-cleaned images were run through DoPHOT, to obtain the positions of the brightest stars, which were then matched (using DAOMATCH and DAOMASTER, Stetson 1992) to obtain the coordinate transformations between epochs. The X and Y offsets were all less than ~ 0.2 arcsec. All the frames for each chip were then shifted by their offsets and median-combined to produce clean and reasonably deep master images, which were then passed through DoPHOT, to produce a master list of objects, retaining only those objects DoPHOT classified as stars. The coordinates of the master list were then transformed to the positions of each epoch, and each of these lists were used within DoPHOT to obtain raw DoPHOT photometry of each of the master list objects in each of the epoch frames.

The raw photometry was then calibrated to equivalent 0.5 arcsec aperture magnitudes, using aperture corrections and measured zero-points (appropriate for long exposures) for both filters and each chip (see Appendix A). The photometry of all epochs for each object, now calibrated to 0.5 arcsec aperture magnitudes, was then combined using DAOMASTER, to produce a light curve for every object in the input master list.

2.2. ALLFRAME

For ALLFRAME, the original science frames were used (i. e. treating each of the cosmic ray-split exposures as two individual epochs), following the ALLFRAME method described for previous galaxies in this series (e. g. Ferrarese et al. 1996; Silbermann et al. 1996). The DAOPHOT/ALLFRAME program (Stetson 1994) takes a different approach in doing the photometry, in that an analytic model of the PSF is augmented by an empirically-determined difference map, which represents the intensity-weighted mean difference between the observed PSF of a large sample of isolated stars and the analytic function. This model of the PSF is also allowed to vary as a quadratic function of position on the chip, to mimic the variations in the true PSF across each chip. In the case of the HST images of NGC 7331, there were too few isolated stars to adequately characterize the PSF, so the model PSFs derived from a number of independent images of globular cluster fields were used. ALLFRAME then fits these model PSFs (one per filter and chip) to all stars on all the frames. To do this, ALLFRAME must first have a master input list of objects, which like DoPHOT, was derived from median images produced from coordinate transformations defined by matches of bright isolated stars on each of the individual cosmic ray-cleaned frames. Unlike DoPHOT, ALLFRAME only uses this star list as a starting point, and uses the results of simultaneous PSF fitting on all the frames to improve the coordinate transformations between frames, thereby iteratively improving the master list. The final photometry files produced by ALLFRAME for each epoch were then matched using DAOMASTER, to produce a single file containing the positions and magnitudes of all the matched stars at all the epochs.

Although cosmic rays are left in each of the single epoch frames, these are generally not a problem, as the position of each star is determined solely from the master list and the coordinate transformation of the entire frame. Thus cosmic rays falling near a star will not affect its centroid, and are rejected as being deviant pixels during the PSF fitting. The only time a cosmic ray will affect the photometry is when it impacts squarely on the peak of the stellar profile, making it appear that the star is unusually bright in that one image. Such defects must be identified and removed at a later stage of the analysis, by comparison with the rest of the lightcurve.

The aperture corrections were determined for each epoch, to allow for focus variations (since unlike DoPHOT, the model PSF was fixed in ALLFRAME). As there were few isolated stars to do this, the

procedure was made more robust by determining a mean set of growth curves for the observed PSFs of isolated stars in each chip/filter from all the Key Project galaxies to date, which were used to derive the 0.5 arcsec aperture magnitudes for the few isolated stars, then measuring the mean epoch aperture correction as the difference between this aperture magnitude and the PSF (ALLFRAME) magnitude. The rms dispersion about the mean for these aperture corrections were less than ~ 0.01 magnitude, except for F814W chip 3, which was 0.02 magnitude. This scatter is insignificant compared to the uncertainties of the individual PSF fits of 0.1 to 0.3 magnitude which are typical of the Cepheids. The mean aperture corrections for each epoch/chip/filter, as well as zero-points appropriate for long exposures, are listed in Appendix A. These were added to the PSF magnitudes of all objects, to obtain 0.5 arcsec magnitudes (F555W_{0.5} and F814W_{0.5}).

2.3. Comparison Between DoPHOT and ALLFRAME Photometry

To allow easier external comparisons with our calibrated magnitudes, we list in Table 2 the positions and calibrated mean ALLFRAME and DoPHOT magnitudes (V and I) of stars which are isolated and unaffected by cosmic ray events, and which DoPHOT classified as stars. Due to crowding, there are not as many of these isolated reference stars as we would have liked.

The calibrated magnitudes (i. e. V and I) differences of these (reference) stars are given in Table 3, and plotted in Figure 3. In the wide field chips (chips 2-4), where the Cepheids are, these reference star magnitudes agree to within 0.05 mag. Some of the scatter between these DoPHOT and ALLFRAME magnitudes arises from the different methods used to fit the model PSF, in that DoPHOT weights each pixel independently by its own noise estimate, whereas ALLFRAME weights relative to its PSF profile. Although the comparison of the Cepheid photometry itself yields better agreement between the two programs, we are continuing to try and understand the source of these remaining differences. In particular, we are undertaking a series of artificial star experiments designed to investigate the effects of crowding, differences in PSF's, the differences in the way the two programs calculate sky values, etc.

An even more relevant comparison, in terms of the distance to NGC 7331, is the difference in the calibrated Cepheid magnitudes (see § 3 and § 4), which is reflected in the difference between the Period-Luminosity fits in Table 7. This indicates that the DoPHOT and ALLFRAME calibrated magnitudes agree to ~ 0.05 mag in V , a difference of less than one sigma with respect to the internal errors, and well within the external errors. In I , the agreement is even better. The difference between the magnitudes for the Cepheids are also plotted in Figure 3 (open symbols).

3. The Cepheids

To detect the variables, the objects in the DoPHOT photometry sets were first grouped into magnitude bins of width 0.5 mag. A variable was then defined as any object with a robust rms-like dispersion (the $F\text{-}\sigma$ parameter, based on the inner range of variability, as described in Hughes 1989, and derived from Hoaglin, Mosteller & Tukey 1983) greater than twice the mean rms of its magnitude bin. Each object was also required to have been matched in at least 10 epochs. These variables were then searched for likely periods between 10 and 80 days, using a program based on the Phase Dispersion Minimization (PDM) algorithm of Stellingwerf (1978), which is based on the Lafler & Kinman (1965) statistic. The main advantage of this method is that it is efficient at detecting periodicity in small epoch samples, and is insensitive to light curve

shape. Simultaneously, the image of each variable was viewed, to ensure it was not a spurious variable caused by a close association with another object, as well as its light curve, to ensure no spurious objects were selected due to noise or cosmic ray events.

For the ALLFRAME photometry sets, variable candidates were identified using two indicators. The first is similar to the χ^2 parameter of Saha & Hoessel (1990), and the second is the color index parameter of Welch & Stetson (1993). Cepheid candidates were identified by visually examining the phased light curves of the variable candidates. Any epochs contaminated by cosmic rays were removed interactively.

The final list of 13 good Cepheids was selected on the basis that each had to appear Cepheid-like in both candidate lists: a Cepheid-like lightcurve (sharp rise, longer decay for those with periods > 20 days, more sinusoid for periods < 20 days); similar periods; similar amplitudes; and colors consistent with being in the instability strip. No Cepheids were found on chip 1, the planetary camera (PC) chip. This is mainly due to the smaller field of view, for which we would expect just 1.1 Cepheids (based on the mean number of Cepheids found in the WF chips, assuming the stellar population is uniform across all chips). We would also expect to find fewer Cepheids on the PC chip as it has smaller pixels, hence it has larger photometric errors at the magnitudes of the Cepheids, compared to the other wide field (WF) chips (errors of 0.25 to 0.6 mag, at magnitudes of 25 to 27 in V , compared to errors of 0.1 to 0.3 mag on the WF chips), resulting in much lower yields of variable candidates due to the $2\text{-}\sigma$ selection. For Cepheids to have made this cut, they would need to have amplitudes greater than ~ 1.0 mag, and only half the Cepheids in Table 6 have such large amplitudes. The F555W_{0.5} and F814W_{0.5} magnitudes at each epoch are listed in Table 4 (DoPHOT) and Table 5 (ALLFRAME, where the cosmic ray-split epoch magnitudes are intensity averaged).

As in other papers in this series, we calculate two estimates of the mean magnitudes of our Cepheids: mean F555W_{0.5} magnitudes derived from unweighted intensity averaged means:

$$\langle \text{F555W}_{0.5} \rangle = -2.5 \log_{10} \left(\frac{1}{N} \sum 10^{-0.4m_i} \right) \quad (1)$$

and phase-weighted magnitudes

$$(\text{F555W}_{0.5})_{\phi} = -2.5 \log_{10} \left(\frac{1}{N} \sum 0.5(\phi_{i+1} - \phi_{i-1}) 10^{-0.4m_i} \right) \quad (2)$$

Since the amplitudes of Cepheids decrease with wavelength, fewer I -band than V -band observations are required to determine mean magnitudes to the same accuracy. The mean I -band magnitudes were estimated based on 4 epochs following the method developed by Freedman (1988) and applied by Ferrarese et al. (1996). This uses the fact that the amplitude in V is almost twice the amplitude in I , hence a well-sampled mean I magnitude $\langle I \rangle_{12}$ (over ~ 12 epochs) will be estimated as

$$\langle I \rangle_{12} = \langle I \rangle_4 + 0.51(\langle V \rangle_{12} - \langle V \rangle_4) \quad (3)$$

where $\langle I \rangle_4$ and $\langle V \rangle_4$ are the intensity averaged I and V magnitudes at those epochs (up to four) where both F555W and F814W images were obtained.

We used the optimized sampling algorithm developed by Freedman et al. (1994a) to choose epochs which obtain good phase coverage over all bright Cepheid periods (i.e. periods between 10 and 60 days), hence there is very little difference between these mean and phase-weighted magnitudes. Maintaining consistency with previous papers in this series, we will use only the phase-weighted magnitudes in deriving distances, and these are listed in Table 6, where the F555W_{0.5} and F814W_{0.5} magnitudes have been

converted to Johnson V and Kron-Cousins I using the Holtzman et al. (1995b) transformations in Appendix A.

In Table 6 we list the parameters for the final sample of 13 Cepheids: ID; WFPC2 chip number; position (both the RA and Dec at equinox J2000, and their X and Y pixel position on each chip); ALLFRAME period; ALLFRAME phase-weighted V magnitude; ALLFRAME $V - I$ color; DoPHOT period; DoPHOT phase-weighted V magnitude; and DoPHOT $V - I$ color. The Cepheids are identified in the WFPC2 field in Figure 2, as well as in more detailed finding charts in Figure 6, and their light curves, phased to the period given in Table 6, are shown in Figure 7. Although V4 appears crowded, and V8 is near a bright star (see Figure 6), they are still retained as their photometric uncertainties are no larger than other stars of similar magnitude, and the near neighbors subtracted cleanly after PSF fitting. The mean difference between the periods of the two DoPHOT and ALLFRAME Cepheid data sets $\Delta\text{Period} = -0.03$ days, with an rms dispersion of 1.27 days.

The Cepheids in Table 6 are marked in the deep I vs $V - I$ color-magnitude diagram (CMD) in Figure 4, derived from the mean magnitudes from all epochs (for clarity, only every 10th star in the CMD is plotted). All of the Cepheids lie in the instability strip. We also plot the locus of the blue plume, red supergiant and red giant branch for Shapley Constellation III, shifted in magnitude and color to match the relative distance and extinction of NGC 7331. The position of the red giant branch locus implies our limiting magnitude is too bright to apply the tip of the red giant branch distance method (e. g. Lee et al. 1993) as a check on our Cepheid distance.

The luminosity function of the blue plume stars (i. e. with $V - I < 0.3$) is plotted in Figure 5. Before incompleteness (at $V > 26$), the slope of the luminosity function is 0.61, similar to that of M81 (0.57; Hughes et al. 1994), and consistent with other late-type galaxies (Freedman 1985). The luminosity function for stars with Cepheid-like colors ($0.5 < V - I < 1.5$) is also plotted in Figure 5, and shows that incompleteness for Cepheids sets in at $V > 27.8$ mag, consistent with our faintest Cepheid in Table 6, which has $\langle V \rangle = 27.4$ (V8). The degree to which crowding and limiting magnitude affects Cepheid completeness is being investigated via artificial star tests by Ferrarese et al. (in preparation).

4. The Distance to NGC 7331

To obtain a Cepheid distance, we follow the methodology of previous papers in this series, and fit V and I PL relations relative to the LMC Cepheids, adopting the distance and reddening to the LMC of 18.5 ± 0.1 mag and $E(V - I) = 0.13$ (i. e. $E(B - V) = 0.10$, $A_V = 3.3E(B - V)$), and use the Cardelli et al. 1989 extinction law $A_I/A_V = 0.7712 - 0.5897/R_V = 0.592$ for $R_V = 3.3$) from Madore & Freedman (1991; hereafter MF91), and fitting the MF91 PL relations, derived from a set of observations of 32 LMC Cepheids:

$$M_V = -2.76(\pm 0.11)[\log(P) - 1.4] - 5.26(\pm 0.05); \quad rms = 0.27 \quad (4)$$

$$M_I = -3.06(\pm 0.07)[\log(P) - 1.4] - 6.09(\pm 0.03); \quad rms = 0.18 \quad (5)$$

to obtain V and I distance moduli (μ_V, μ_I) .²³

As can be seen in the image of Figure 2 (and to a more dramatic extent in Figure 1), there are noticeable amounts of dust in NGC 7331, so it is important to measure and account for this as accurately as possible. As in MF91, we measure the mean reddening $E(V - I)$ for the whole sample of Cepheids from the difference $\mu_V - \mu_I$, which is then used to derive the extinction-corrected distance.

We have two methods of measuring apparent distance moduli in V and I . The first adopts the LMC PL relations of MF91, using least squares fits with slopes fixed at the MF91 values. The second method is that used by Ferrarese et al. (1996) for M100. This assumes nothing about the slopes of PL relations, but simply adds a common magnitude offset to the set of LMC Cepheids with periods greater than 10 days used by MF91, such that when their magnitudes are combined with the NGC 7331 Cepheids, the scatter of the combined set is minimized. The final offset is then the difference in apparent distance modulus between the LMC and NGC 7331. Both methods produced virtually identical results, and so we only present the results of the first method. The PL relations are shown in Figures 8 and 9, where the fits using the MF91 slopes are the solid lines, with the dotted lines being the $2\text{-}\sigma$ ridge lines (i.e. 95% confidence interval).

The number of Cepheids used in the fits, the apparent distance moduli in V and I (μ_V, μ_I) , reddenings $E(V - I)$, and extinction-corrected distance moduli μ_0 for each photometry set are listed in Table 7. The $1\text{-}\sigma$ uncertainties in μ_V and μ_I are internal errors, being the standard errors of the mean from the least squares fits (combined in quadrature with the uncertainties in the LMC PL fits). Because a component of the scatter in the V and I PL relations will be correlated, the uncertainty in μ_0 is derived from the dispersion in a Wesenheit function, $W = V - 2.45(V - I)$, which is adapted to the reddening assumed between V and I , as this will implicitly propagate the photometric uncertainties and cancels the differential reddening-induced scatter (Madore 1982). The uncertainty in μ_0 in Table 7 thus includes the observational uncertainties in the photometry. Ideally we would like to search for any possible zero-point variations between chips, but with so few Cepheids it would be impossible to tell if any differences were due to a zeropoint variation or simply a statistical fluctuation. For the record, for chips 2 and 4, the μ_V were within $1.5\text{-}\sigma$ of the all chip mean for ALLFRAME and DoPHOT, but the chip 3 μ_V was $3\text{-}\sigma$ larger for ALLFRAME and $4\text{-}\sigma$ larger for DoPHOT. The luminosity function for stars with Cepheid-like colors in Figure 5 showed that we may be affected by incompleteness at the faintest (i. e. short period) end of the Cepheid distribution. To check for the effects this may have in fitting the PL relations, the lower period limit was also varied, from 10 days (the lower period limit) to 15, 20, and 25 days (Table 7). All fluctuations in μ_0 relative to the all-Cepheid fit are within the uncertainties, and there is no strong systematic trend in μ_0 , as the low period limit is increased from 10 to 25 days. This is due to our keeping the slope of the

²³Tanvir (1996) has re-derived the LMC PL relations, from a compilation of data from several sources, of 53 LMC Cepheids, and finds they are best fit by PL relations of the form:

$$M_V = -2.774(\pm 0.083)[\log(P) - 1.4] - 5.262(\pm 0.040); \quad rms = 0.233$$

$$M_I = -3.039(\pm 0.059)[\log(P) - 1.4] - 6.049(\pm 0.028); \quad rms = 0.164$$

There is very little difference in the V PL relation, but a significant difference in the I PL relation zero-point. Tanvir has attributed this difference to the fact that for the Cepheids in Martin, Warren & Feast (1979), MF91 used I magnitudes derived from $\langle V \rangle - \overline{V - I}$ (where $\overline{V - I}$ is the mean of the $V - I$ colors at all epochs), rather than intensity means of the I data. For Cepheids of normal amplitudes, this creates systematic errors of 0.02-0.09 mag. If confirmed, this means that use of the MF91 relations would produce a systematic overestimate of the relative I distance modulus of a galaxy by ~ 0.04 mag, hence of the reddening, which produces an overestimate of the extinction-corrected distance modulus of 0.1 mag, and a corresponding underestimate of H_0 by 5%. An ongoing program to measure mean I -band magnitudes for a sample of LMC Cepheids being carried out by us at Las Campanas Observatory and Mount Stromlo will shed further light on this issue. In the meantime, to be consistent with previous papers in this series, we continue to use the MF91 PL relations.

PL relation fixed, and indicates that no strong Malmquist bias is present in our Cepheid sample. Thus our distance estimate will not be significantly affected by incompleteness.

The distance moduli derived from the all-Cepheid sample for ALLFRAME and DoPHOT agree within one sigma, indicating no significant difference between the two procedures. We note that the DoPHOT distance modulus for periods above 15 days agrees very well with the ALLFRAME result, as would be expected given the higher signal to noise ratio of these brighter Cepheids. For consistency with previous papers, and for simplicity, we henceforth quote the results based on the ALLFRAME photometry alone.

The reddening of $E(V - I) = 0.19$ (ALLFRAME), implies a mean extinction to NGC 7331 of $A_V = 0.47 \pm 0.20$ mag.²⁴ The foreground Galactic extinction in the direction of NGC 7331 is $A_V = 0.27$ (derived from $E(B - V) = 0.083$ from Burstein & Heiles 1984), thus the mean extinction internal to the NGC 7331 Cepheid field is 0.20 mag in V . The extinction-corrected distance modulus is 30.89 mag, equivalent to a distance of 15.1 Mpc.

4.1. Errors in the Distance Modulus

The various contributions to the total error budget are listed in Table 8. In addition to the uncertainties of the photometry (included in the PL fits), the true distance estimate will also be affected by the systematic uncertainties in the zero-point calibration from HST to ground-based V and I magnitudes, and the LMC distance modulus. The former are assumed to be uncorrelated, and hence must be factored for the ratio of their contributions via the extinction correction: i. e. $\mu_0 = 2.45\mu_I - 1.45\mu_V$, hence $\Delta(ZP) = ((2.45\Delta(ZP)_I)^2 + (1.45\Delta(ZP)_V)^2)^{\frac{1}{2}}$.

Differences in metal abundance between our field in NGC 7331 and the calibrating Cepheids in the LMC might affect our derived distance. Both the empirical test in M31 performed by Freedman & Madore (1990), and the theoretical calculations of Chiosi, Wood, & Capitanio (1993), suggested that the magnitude of such a dependence is relatively weak. On the other hand, Gould (1994), using the same data as Freedman & Madore (1990), but employing a different method of analysis, claimed a sizable effect of $\Delta\mu \sim 0.6\Delta[\text{Fe}/\text{H}]$, although there were inconsistencies between different bands. Stiff (1995) also used the Freedman & Madore (1990) data, in yet another analysis, and found a similarly sized effect as found by Gould (1994). Apart from the different methodologies used, much of the disparity between these three studies, based as they are on identical data (38 Cepheids in M31, spanning a range of metallicity $\Delta[\text{Fe}/\text{H}] = 0.75$), is due to the differing ways in which the reddening is measured (the effects of reddening and metallicity both act in the same color direction), and is partly due to the small number of Cepheids in the metal poor field (only eight), and to the fact that M31 has reasonably large amounts of reddening which must be corrected. More recently, Sasselov et al. (1997) find evidence for an intermediate metallicity dependence ($\Delta\mu \sim 0.4\Delta[\text{Fe}/\text{H}]$) between the LMC and SMC Cepheids. Although this study enjoys a surplus of Cepheids (500), it also suffers from inherent uncertainties due to the smaller range in metallicity ($\Delta[\text{Fe}/\text{H}] = 0.35$), plus extra uncertainties due to the unknown distance between the LMC and SMC, and the considerable depth distribution for the SMC Cepheids. To sidestep most of these uncertainties, we have made an empirical test of the metallicity dependence of the PL relation, based on observations of two fields

²⁴We thank the referee for pointing out that extinctions should formally be calculated in the observed passbands. However, for stars of Cepheid-like colors this makes very little difference. Using the mean extinction values derived from Tables 12a and 12b of Holtzman et al. (1995b) for $E(B - V) = 0.15$ (i.e. $E(V - I) = 0.19$), then $A_{F555W} = 0.46$, almost identical to the value for A_V , and well within the observational uncertainties.

in M101 (Kennicutt et al. 1998). These samples in M101 have the advantage of spanning a much larger range of metallicity ($\Delta[\text{Fe}/\text{H}] = 1.4$; Zaritsky et al. 1990), while also having reduced reddening due to M101 being almost face-on. The empirical metallicity dependence is $\Delta\mu = 0.24(\pm 0.16)\Delta[\text{O}/\text{H}]$, in the sense that a target sample of Cepheids more metal rich than the LMC would appear to be closer than it actually is, and $\Delta[\text{O}/\text{H}]$ is the difference in $[\text{O}/\text{H}]$ abundance, in dex, between the target galaxy and the LMC.

As argued in Kennicutt et al. (1998), a metallicity effect of this magnitude is barely detectable in the metallicity range of our Key Project galaxies. In particular, for NGC 7331, the H II region abundances measured by Oey & Kennicutt (1993) and Zaritsky, Kennicutt, & Huchra (1994), and recently supplemented by our own measurements of an H II region in the Cepheid field itself, indicate an oxygen abundance of about 1.5 ± 0.3 times that of the LMC, which would correspond to a correction of only $+0.05 \pm 0.04$ mag in distance modulus. Given the small size of the effect and its large uncertainty, and in order to be consistent with previous galaxies in this series, we have not applied it to our data, but simply add this as a possible systematic error in Table 8. Once the Cepheid distances to all Key Project galaxies have been obtained, we intend using the combined data set, with its large range in metallicity, to reduce the uncertainty in the metallicity effect, and apply it to all galaxies prior to calibrating the secondary distance indicators.

4.2. Comparison with Previous Distance Estimates

Previously published distance estimates to NGC 7331 are listed in Table 9. Sersic (1960) and Osman (1982) used the size distributions of H II regions and dust clouds, respectively, to estimate distances, and van den Bergh (1960) used a calibration of luminosity classes. Rubin et al. (1965) estimated a velocity distance of 14.4 Mpc derived from a recession velocity of +1082 km/s (corrected only for Galactic rotation) and assuming $H_0 = 75$ km/s/Mpc. They also noted the similarities between M31 and NGC 7331, and by assuming similar diameters, made a further distance estimate in terms of the ratio of their apparent diameters (20:1). This estimate converts to 15.4 Mpc, where we adopt the distance to M31 of 770 kpc from Freedman & Madore (1990). Balkowski et al. (1973) used a variety of correlations between estimators of mass, luminosity, morphology, and H I density, to derive a mean distance estimate, with a large scatter, of 13_{-5}^{+9} Mpc. Tully (1988) estimated a velocity distance of 14.3 Mpc based on assuming $H_0 = 75$ km/s/Mpc, and a Virgo-centric infall model of the Local Group of 300 km/s, while the velocity data of Aaronson et al. (1982a), when coupled with the Virgo model of Aaronson et al. (1982b), imply a distance of 12 Mpc. The only explicit Tully-Fisher distance estimate for NGC 7331 is in the B band, and is 9.6 Mpc (Bottinelli et al. 1985). However, Aaronson et al. (1982a) published the IRTF parameters ($H_{-0.5}$ and $\Delta V(0)$) for NGC 7331, which converts to an IRTF distance of $10.1_{-1.7}^{+2.0}$ Mpc, using the calibration of Aaronson, Mould & Huchra (1980) (i.e. $H_{-0.5}^{abs} = -21.23 - 10.0[\log\Delta V(0) - 2.5]$, $\sigma = 0.4$). Using the same calibration, Aaronson & Mould (1983) derived a distance to the NGC 7320/7331 pair of $12.9_{-2.8}^{+3.5}$ Mpc.

The only recorded supernova in NGC 7331 was SN1959D, of type III, unfortunately occurring before the era of estimating distances to type II supernovae from the expanding photospheres method (e. g. Schmidt et al. 1994²⁵).

²⁵Although Schmidt et al. list SN1989L as occurring in NGC 7331, this should read NGC 7339.

5. Discussion

The aim of the Key Project is the measurement of the Hubble Constant by calibration of secondary distance indicators. We consider the impact of our new distance on the calibration of two such distance indicators here.

5.1. The Tully Fisher relation

Mould et al. (1996) have updated the calibration of the infrared Tully Fisher (IRTF) relation, noting the importance of populating the calibration for galaxies of large line width, as these are galaxies which can be detected at large distances, where peculiar velocities are negligible relative to recession velocities. In Table 10 and Figure 10 we add NGC 7331 to the TF calibration derived from all suitable galaxies which now have Cepheid distances. We use the H_g magnitudes of Tormen & Burstein (1995), which are the Aaronson et al. (1982a) $H_{-0.5}$ magnitudes re-calculated to agree with the optical diameters in RC3, and which do not include any corrections for inclination. For any given galaxy, the major effect of these changes is that the H_g magnitudes are about 0.35 magnitudes brighter than the $H_{-0.5}$ magnitudes. We adopt an H I velocity width of 531 ± 10 km/s (given by Fisher & Tully), an inclination for NGC 7331 of 73° , in agreement with Tormen & Burstein (1995), but 2° less than that of Aaronson et al. (1982a).

The least squares fit IRTF relation excluding NGC 7331 is $H_g = -9.6(\pm 2.4)(\log \Delta V - 2.5) - 21.7(\pm 0.3)$, with $\sigma = 0.35$ (the dashed-dotted line in Figure 10). When we add in NGC 7331 the fit becomes $H_g = -10.2(\pm 2.2)(\log \Delta V - 2.5) - 21.8(\pm 0.3)$, with $\sigma = 0.39$ (the solid line in Figure 10). Hence this distance to NGC 7331 is consistent with the current IRTF calibration, but it points to a dispersion approaching 0.4 mag in the relation, not very different from that found by Aaronson & Mould (1983) in groups and clusters. Such a dispersion is highlighted by the fact that although NGC 7331 and M31 have very similar line widths and diameters, NGC 7331 is one magnitude brighter in H_g , implying an M/L lower by a factor of ~ 2.5 , possibly due to a different star formation history.

The Tully-Fisher relation is a dynamical relation, and improved understanding of the kinematics and mass to light ratio of the calibrator galaxies can contribute to developing the relation. The kinematics of NGC 7331 have been extensively analyzed by Bower et al. (1993), who were able to fit a constant M/L_V dynamical model, as a function of radius, and found $M/L_V = 5.3$, assuming a distance of 12 Mpc (from Aaronson et al. 1982a). Our new distance therefore implies an $M/L_V = 4.2$, and a total mass of $4.6 \times 10^{11} M_\odot$. This is comparable to a mass derived from Fisher & Tully (1981) of $4.0 \pm 0.5 \times 10^{11} M_\odot$, and $M/L_B = 7.9$ (where our distance of 15.1 Mpc implies a Holmberg diameter $A_H = 65$ kpc, $\mu_0 = 30.88$ implies $M_B = -21.38$ and $\log L_B = 10.74$).

Although NGC 7331 looks like a normal early-intermediate type spiral galaxy with a significant bulge, it is also claimed to have a mildly active (weak LINER) nucleus. Cowan et al. (1994) measured its 20 cm and 6 cm radio flux to be 234 and 121 μJy , respectively. At a distance of 15.1 Mpc, this makes it 3.3 and 4.6 times the luminosity of Sgr A, at these wavelengths. However, Ohya & Taniguchi (1996) suggest, on the basis of stellar population synthesis, that the apparent nuclear activity in NGC 7331 is due to a recent burst of star formation, rather than an active galactic nucleus.

5.2. Surface Brightness Fluctuations

In addition to the TF calibration, the large bulge in NGC 7331 can be used as a calibrator for the surface brightness fluctuations (SBF) method. Tonry et al. (1997) have adopted a SBF calibration of

$$\overline{M_I} = \overline{M_{I0}} + 4.5 (V - I - 1.15) \quad (6)$$

At a distance of 15.1 Mpc, their measurement of a field 1-2 arcmin along the minor axis of NGC 7331 yields $\overline{M_{I0}} = -2.3 \pm 0.3$ mag, significantly brighter than their adopted value of -1.74 ± 0.07 mag derived from the mean calibration (Tonry et al. 1997). The distance to NGC 7331 from the Cepheids and SBF methods thus disagree by 0.55 magnitude. At least part of this disagreement is probably due to internal reddening in the NGC 7331 bulge field. Although Tonry et al. take into account the foreground reddening to each of the SBF samples (e. g. $A_B = 0.33$ mag for NGC 7331), no correction is made for any internal extinction. For the E and S0 galaxies, and the very edge-on spirals, this may be appropriate, but for NGC 7331 there is evidence from stellar population studies in the bulge by Prada (1996) that there is additional reddening internal to the bulge, implying an extinction of $A_V \sim 0.5$ mag, or $A_I = 0.3$ mag. A quirk of SBF is that taking reddening into account causes $\overline{M_{I0}}$ to become fainter. Hence an extra reddening of $A_I = 0.3$ would increase the value of $\overline{M_{I0}}$ quoted here, making it more consistent with Tonry’s standard value. As well, if there is this much dust in the bulge of NGC 7331, then it may also have a young stellar component as well. Although the color term in the SBF calibration is intended to allow for such variations, the reddening would tend to mask the bluer colors such a young component would contribute, thus making the deviation from an unreddened old population even greater. These are only possibilities, of course. A larger sample of SBF calibrators will allow us to search for hidden variables in the calibration, just as it does for Tully-Fisher.

5.3. The NGC 7331 Group

According to Garcia (1993), NGC 7331 is the dominant member of a group with three other galaxies: UGC12082, NGC 7320A, and UGC12060, which, relative to NGC 7331, are all within a radius of 1.7° on the sky and within 62 km/s in radial velocities. Garcia also claimed NGC 7363 to be a member of this group, as its heliocentric velocity is 830 km/s in RC3, but Wegner, Haynes & Giovanelli (1993) measure its H I velocity as 6722 km/s, and thus a member of the Pisces-Perseus ridge or super cluster (along with various other galaxies which are nearby, on the sky, such as NGC 7320B, NGC 7320C, NGC 7335, NGC 7337, NGC 7369, and NGC 7340). Our group selection is based on a compilation of all galaxies within a radius of 9 degrees of NGC 7331 (at the distance of NGC 7331, 9 degrees corresponds to 2.4 Mpc), derived from a combination of the CfA Redshift Catalog (Huchra 1997) and the NASA Extragalactic Database. They are listed in Table 11, which gives their name, position (RA and Dec at J2000), galactocentric velocity, and radius on the sky (in degrees, relative to NGC 7331). The group has a velocity dispersion of 64 km s⁻¹ (it might be argued that NGC 7292 and NGC 7217 should be excluded, as the remaining galaxies would then have a velocity dispersion of only 44 km s⁻¹). NGC 7331 is the brightest galaxy in this small group of 8-10 members. The second brightest galaxy is NGC 7217, about 6 degrees away. At 15 Mpc, 6 degrees is only about 1.5 Mpc. NGC 7457 is the third brightest member, and almost all the other galaxies in the group are more than three magnitudes fainter than NGC 7331. This is a moderately isolated group, almost opposite Virgo, and almost 90 degrees away from Fornax, hence its well determined mean velocity of 1110 ± 20 km s⁻¹ (or 1088 ± 16 km s⁻¹ without NGC 7292 and NGC 7217) should provide a stable point of reference in

studying local velocity flows.

6. Conclusion

We have used 15 epochs of HST F555W frames to produce light curves of all stars within the field, to a limiting magnitude of $V \sim 28$ mag, using two photometry programs (DoPHOT and DAOPHOT/ALLFRAME), and from these light curves identified a total of 13 reliable Cepheids in NGC 7331. Using the ALLFRAME data, and an additional 4 epochs of F814W frames, period-luminosity relations derived from LMC Cepheids were fitted to the NGC 7331 Cepheids, to measure a mean reddening of $E(V - I) = 0.18 \pm 0.06$, and an extinction-corrected distance modulus of 30.89 mag (uncertain to ± 0.16 mag (random) and $+0.05 \pm 0.13$ mag (systematic)), equivalent to a distance of $15.1_{-1.3}^{+1.4}$ Mpc.

We are indebted to the staff at STScI for their very able support, in particular to Doug Van Orsow. We also thank John Tonry for early access to the SBF results, and the referee for the helpful comments and suggestions which have clarified many parts of the paper. Support for this work was provided by NASA through grant number 2227-87A from STScI which is operated by AURA under NASA Contract NAS5-26555, and by a NATO Collaborative Research Grant CRG960178. This research has made use of the NASA/IPAC Extragalactic Database (NED) which is operated by JPL, California Institute of Technology, under contract with NASA.

A. Appendix A - Calibration Parameters

There are several differences between DoPHOT and DAOPHOT/ALLFRAME in the way the frames are prepared and PSF fitting is done for each filter set. In DoPHOT the frame pairs are first combined to remove cosmic rays; the width and elongation of an analytic PSF is determined for each frame, but does not vary across a frame; this is compensated by measuring aperture corrections which vary across the frame, but do not vary from frame to frame. In contrast, and as the name implies, ALLFRAME measures the PSF magnitude of all frames; the PSF fitted is a combination of an analytic function and a residual map, both of which are allowed to vary across each frame; and aperture corrections do not vary across each frame (they are also allowed to vary from frame to frame if there are enough isolated stars, but this was not the case for NGC 7331). As well as these differences in measuring instrumental photometry, there are also differences in calibration.

The calibration of the raw DoPHOT photometry is described in detail in Saha et al. (1996). This calibration procedure has been applied systematically to all DoPHOT photometry in this Key Project series, and is given by:

$$\text{HST}_{0.5} = \text{DoPHOT}_{\text{obs}} + 30.0 + AC + 2.5 * \log_{10}(t) + ZP \tag{A1}$$

where $\text{HST}_{0.5}$ mag is the $0''.5$ aperture magnitude system (F555W $_{0.5}$ and F814W $_{0.5}$), as defined by Holtzman et al. (1995b), AC is the aperture correction (to correct for the 9×9 pixel square aperture, derived from observations of Leo I), t is the exposure time, in seconds, and ZP is the zero-point, derived from comparing magnitudes obtained from the first epoch NGC 7331 frame with observations of Pal 4, following the prescription of Holtzman et al. (1995b).

The DoPHOT aperture corrections are given by:

$$AC = C0 + C1 * x + C2 * y + C3 * x * x + C4 * y * y + C5 * x * y \tag{A2}$$

where x and y are the pixel coordinates of each full (800×800) WFPC2 chip, and the C coefficients are given in Table A1 (the C0 coefficients also contain an additional offset derived by measuring a mean aperture correction from the first epoch of the NGC 7331 frames).

As the calibration to $\text{HST}_{0.5}$ mag is done via cluster data, which have a faint background, these were corrected for the CTE effect, by adding a mean correction of -0.02 mag, which is an approximation to the recommended correction in Holtzman et al. (1995b) (which is to apply a ramp of $-0.04\text{mag}/800$ Y pixels). As discussed in Hill et al. (1998), zero-points for WFPC2 also seem to differ by 0.05 mag between short and long exposures (i. e. objects observed with long exposure times appear brighter by 0.05 mag, compared to short exposure times). For long exposures (i. e. ours) the DoPHOT zero-points (for a gain of 7) are defined in Table A2.

Because DoPHOT and DAOPHOT have different methods of estimating the sky and fit different PSF profiles, their calibration to standard magnitudes has to be done independently. To gain full advantage of this effort, the ALLFRAME calibration was also done using a different data set, based on exposures of stars in Galactic globular clusters, to provide an independent check on the calibration procedure. Because ALLFRAME allows the PSF to vary across each chip, its calibration only requires zero-points and a single aperture correction per chip/filter to convert the raw magnitudes to equivalent 0.5 arcsec aperture magnitudes, where for DAOPHOT/ALLFRAME:

$$\text{HST}_{0.5} = \text{ALLFRAME}_{\text{obs}} + AC + 2.5 * \log_{10}(t) + ZP \quad (\text{A3})$$

The zero-points were derived for each chip and filter from weighted averages of long exposure HST vs ground-based photometry of the clusters NGC 2419 and Pal 4 (Bolte & Stetson, private communication). A mean CTE ramp effect of 0.040 mag/800 pixels was measured, and was then applied to the input cluster magnitudes. Mean aperture corrections for each chip/filter combination were derived from curve of growth models derived from fits to isolated stars in each of the Key Project galaxies. These, and the zero-points for ALLFRAME (again, on the LONG exposure scale) are given in Table A2.

The HST magnitudes were then transformed to Johnson V or Kron-Cousins I magnitudes, using the transformations derived by Holtzman et al. (1995b):

$$V = \text{F555W}_{0.5} - 0.045(V - I) + 0.027(V - I)^2 \quad (\text{A4})$$

$$I = \text{F814W}_{0.5} - 0.067(V - I) + 0.025(V - I)^2 \quad (\text{A5})$$

where the $(V - I)$ colors were estimated from iteration, starting from $\text{F555W}_{0.5} - \text{F814W}_{0.5}$, and ending when $|V - I - (V - I)| < 0.001$ mag (usually one iteration was sufficient).

REFERENCES

- Aaronson, M., Mould, J., & Huchra, J. 1980, *ApJ*, 237, 655
- Aaronson, M., et al. 1982a, *ApJS*, 50, 241
- Aaronson, M., et al. 1982b, *ApJ*, 258, 64
- Aaronson, M., & Mould, J. R. 1983, *ApJ*, 265, 1
- Balkowski, C., et al. 1973, *â*, 25, 319
- Begeman, K. G. 1987, PhD thesis, University of Groningen *MNRAS*, 249, 523
- Bottinelli, L., et al. 1985, *A&AS*, 59, 43
- Bower, G. A., Richstone, D. O., Bothun, G. D., & Heckman, T. M. 1993, *ApJ*, 402, 76
- Burstein, D., & Heiles, C. 1984, *ApJS*, 54, 33
- Cardelli, J. A., Clayton, G.C., & Mathis, J.S. 1989, *ApJ*, 345, 245
- Chiosi, C., Wood, P. R., & Capitanio, N. 1993, *ApJS*, 86, 541
- Cowan, J. J., Romanishin, W., & Branch, D. 1994, *ApJ*, 436, L139
- de Vaucouleurs, G., de Vaucouleurs, A., Corwin, H., Buta, R., Paturel, A., & Fouqué, P. 1991, in *Third Reference Catalog of Bright Galaxies*, (Berlin: Springer) (RC3) ESA SP-310
- Ferrarese, L. et al. 1996, *ApJ*, 464, 568
- Fisher, J. R., & Tully, R. B. 1981, *ApJS*, 47, 139
- Freedman, W. L. 1985, *ApJ*, 299, 74
- Freedman, W. L. 1988, *ApJ*, 326, 691
- Freedman, W. L. 1990, *ApJ*, 355, L35
- Freedman, W. L., & Madore, B. F. 1990, *ApJ*, 365, 186
- Freedman, W. L., et al. 1994a, *ApJ*, 427, 628
- Freedman, W. L., et al. 1994b, *Nature*, 371, 757
- Garcia, A. M. 1993, *A&AS*, 100, 47
- Gould, A. 1994, *ApJ*, 426, 542
- Graham, J. A., et al. 1997, *ApJ*, 477, 535
- Hill, R. J., et al. 1998, *ApJ*, in press
- Hoaglin, D. C, Mosteller, F., & Tukey, J. W. 1983, in *Understanding Robust and Exploratory Data Analysis*, (New York: Wiley)
- Holtzman, J. A., et al. 1995a, *PASP*, 107, 156
- Holtzman, J. A., et al. 1995b, *PASP*, 107, 1065
- Huchra, J. 1997, CfA Redshift Catalog, private communication
- Huchtmeier, W. K., & Richter, O. -G. 1989, in *A General Catalog of H I Observations of Galaxies*, (New York: Springer)
- Hughes, S. M. G. 1989, *AJ*, 97, 1634
- Hughes, S. M. G. et al. 1994, *ApJ*, 428, 143

- Hughes, S., Han, M., & Hoessel, J. 1996, in *Science with HST - II*, eds. P. Benvenuti, F. D. Macchetto, & E. J. Schreier (ESA/NASA Publication), p46
- Kelson, D. D. et al. 1996, *ApJ*, 463, 26
- Kennicutt, R. C., Freedman, W. L., & Mould, J. R. 1995, *AJ*, 110, 1476
- Kennicutt, R. C., et al. 1998, *ApJ*, submitted
- Lafler, J., & Kinman, T. D. 1965, *ApJS*, 11, 216
- Lee, M. G., Freedman, W. L., & Madore, B. F. 1993, *ApJ*, 417, 553
- Madore, B. F., & Freedman, W. L. 1991, *PASP*, 103, 933 (MF91)
- Madore, B. F. 1982, *ApJ*, 253, 575
- Marcelin, M., Petrosian, A. R., Amram, P., & Boulesteix, J. 1994, *A&A*, 282, 363
- Martin, W. L., Warren, P. R., & Feast, M. W. 1979, *MNRAS*, 188, 139
- Mould, J., Sakai, S., Hughes, S., & Han, M. 1996, in *Proceedings of the STScI May Symposium on the Extragalactic Distance Scale* (Cambridge: Cambridge University Press), p158
- Oey, M. S., & Kennicutt, R. C. 1993, *ApJ*, 411, 137
- Ohyama, Y., & Taniguchi, Y. 1996, in *ASP Conf Ser 103, The Physics of Liners in View of Recent Observations*, eds. M. Eracleous, A. Koratkar, C. Leitherer, and L. Ho, p205
- Osman, A. M. I., Ella, M. S., & Issa, I. A. 1982, *AN*, 303, 329
- Phelps, R., et al. 1998, *ApJ*, submitted
- Prada, F. 1996, private communication
- Rawson, D. M., et al. 1997, *ApJ*, 488, 000
- Rubin, V. C., Burbidge, E. M., Burbidge, G. R., Crampin, D. J., & Prendergast, K. H. 1965, *ApJ*, 141, 759
- Saha, A., & Hoessel, J. G. 1990, *AJ*, 99, 97
- Saha, A., et al. 1994, *ApJ*, 425, 14
- Saha, A., et al. 1996, *ApJ*, 466, 55
- Sandage, A., & Tammann, G. 1981, in *A Revised Shapley-Ames Catalog of Bright Galaxies*, (Washington DC: Carnegie Institution of Washington)
- Sasselov, D. D., et al. 1997, *A&A*, in press
- Schechter, P. L., Mateo, M., & Saha, A. 1993, *PASP*, 105, 1342
- Schmidt, B. P., et al. 1994, *ApJ*, 432, 42
- Sersic, J. L. 1960, *Z.f.Astrophys.*, 50, 168
- Silbermann, N. A., et al. 1996, *ApJ*, 470, 1
- Stellingwerf, R. F. 1978, *ApJ*, 224, 953
- Stetson, P. B. 1992, in *Stellar Photometry – Current Techniques and Future Developments*, IAU Coll. 136, eds. C. J. Butler and I. Elliot, p. 291
- Stetson, P. B. 1994, *PASP*, 106, 250
- Stift, M. J. 1995, *A&A*, 301, 776
- Tanvir, N. R., et al. 1995, *Nature*, 377, 27

- Tanvir, N. R. 1996, Proceedings of the STScI May Symposium on the Extragalactic Distance Scale, (Cambridge: Cambridge University Press), in press
- Tonry, J. L., Blakeslee, J. P., Ajhar, E. A., & Dressler, A. 1997, *ApJ*, 475, 399
- Tormen, G., & Burstein, D. 1995, *ApJS*, 96, 123
- Tully, R. B. 1988, *Nearby Galaxies Catalog*, (Cambridge: Cambridge University Press)
- van den Bergh, S. 1960, *Public. David Dunlap Observatory*, 2, #6
- Wegner, G., Haynes, M. P., & Giovanelli, R. 1993, *AJ*, 105, 1251
- Welch, D. L., & Stetson, P. B. 1993, *AJ*, 105, 1813
- Westerlund, B. E. 1997, *The Magellanic Clouds*, Cambridge Astrophysics Series: 29, (Cambridge: Cambridge University Press)
- Zaritsky, D., et al. 1990, *AJ*, 99, 1108
- Zaritsky, D., Kennicutt, R. C., & Huchra, J. P. 1994, *ApJ*, 420, 87

Figure Captions

Fig. 1.— A 9.5×9.5 arcmin V image of NGC 7331, obtained with the Prime Focus TEK camera on the Isaac Newton Telescope, La Palma. The position of the WFPC2 field is indicated by the chevron, and the position of SN1959D is also marked. North is to the RIGHT, and East is UP (for purely aesthetic reasons). The background galaxies to the east are (from south to north) NGC 7337, NGC 7335, and NGC 7336.

Fig. 2.— An F555W medianed image of the WFPC2 mosaic (with North UP, East to the LEFT). The positions of the Cepheids in Table 6 are marked by labeled circles.

Fig. 3.— Comparison of calibrated V and I photometry of the reference stars from chips 2-4 in Table 2 (filled symbols) and the Cepheids in Table 6 (open symbols). Circles, triangles, and squares are stars from chips 2, 3, and 4, respectively.

Fig. 4.— I vs $V - I$ color-magnitude diagram for all chips, using the calibrated ALLFRAME photometry (for clarity, only every tenth star is plotted). Also shown are the Cepheids from Table 6 (filled circles), which all lie within the instability strip. The three lines represent the locus of the blue plume and red giant and supergiant branches of Shapley Constellation III in the LMC, shifted to the distance and reddening of NGC 7331.

Fig. 5.— The solid curve is the V luminosity function for all stars with $V - I < 0.3$ (ALLFRAME magnitudes), representing the blue plume. The dashed line is a least squares fit to this luminosity function between $V = 23$ and $V = 26$ mag. The dotted curve is the V luminosity function for all stars with $0.5 < V - I < 1.5$ (ALLFRAME magnitudes).

Fig. 6.— Finding charts for each Cepheid listed in Table 6. Each chart is centered on the Cepheid, and is 4×4 arcsec squared (i. e. 40×40 WF pixels). North is up, east to the left.

Fig. 7.— Light curves, phased to the relevant period, for each Cepheid listed in Table 6. On the left are the calibrated DoPHOT magnitudes, on the right are the calibrated ALLFRAME magnitudes.

Fig. 8.— V (upper panel) and I (lower panel) PL relations for the Cepheids listed in Table 6 (calibrated ALLFRAME magnitudes). The NGC 7331 Cepheids are the solid circles, and the LMC Cepheids are the open circles. The solid lines are least squares fits with the MF91 fixed slopes, and the dotted lines are the 95% confidence interval (i.e. the $2\text{-}\sigma$ ridge lines).

Fig. 9.— V (upper panel) and I (lower panel) PL relations for the Cepheids listed in Table 6 (calibrated DoPHOT magnitudes). Symbols and lines as per Figure 8.

Fig. 10.— IRTF absolute calibration, with absolute H_g magnitudes vs $\log(\Delta V) - 2.5$, from data in Table 10. Filled circles are the galaxies used by Freedman (1990), filled squares are the galaxies with recent HST-derived Cepheid distances, and the filled star is NGC 7331. The dashed line is a least squares fit solution to the Freedman (1990) set of galaxies, the dashed-dotted line is a least squares fit solution to all but NGC 7331, and the solid line is the least squares solution including NGC 7331 (see text).

Table 1. Epochs of Observations.

Epoch	Julian Date	Filename	Date	Exposure times (sec)		Filter
1	2449521.832	u2781q01t	18/06/94	1200	1600	F555W
2	2449530.612	u2781r01t	27/06/94	1200	1600	F555W
3	2449543.952	u2781t01t	10/07/94	1200	1600	F555W
4	2449545.762	u2781u01t	12/07/94	1200	1600	F555W
5	2449549.586	u2781v01t	16/07/94	1200	1600	F555W
6	2449552.806	u2781w01t	19/07/94	1200	1600	F555W
7	2449557.044	u2781x02t	24/07/94	1200	...	F555W
8	2449561.927	u2781y01t	28/07/94	1200	1600	F555W
9	2449573.584	u2781s01t	9/08/94	1200	1600	F555W
10	2449573.861	u2782001t	9/08/94	1200	1600	F555W
11	2449581.226	u2782101t	17/08/94	1200	1600	F555W
12	2449887.615	u2o30101t	19/06/95	1200	1600	F555W
13	2449902.628	u2o30201t	4/07/95	1200	1600	F555W
14	2449921.593	u2o30301t	23/07/95	1200	1600	F555W
15	2449946.395	u2o30401t	17/08/95	1200	1600	F555W
1	2449521.966	u2781q03t	18/06/94	1200	1600	F814W
2	2449530.746	u2781r03t	27/06/94	1200	1600	F814W
9	2449567.754	u2781z06t	3/08/94	1200	...	F814W
12	2449887.631	u2o30103t	19/06/95	1200	1600	F814W
13	2449902.645	u2o30203t	4/07/95	260	...	F555W
13	2449902.650	u2o30204t	4/07/95	260	...	F814W

Table 2. Reference Star Photometry.

ID	Chip	RA (J2000)	Dec	X	Y	V_{Alf}	I_{Alf}	V_{Doph}	I_{Doph}
R 1	1	22:37:01.47	+34:28:10.2	206.2	100.1	24.14 ± 0.08	23.83 ± 0.23	24.43 ± 0.09	23.62 ± 0.61
R 2	1	22:37:00.40	+34:28:09.0	211.7	394.2	21.91 ± 0.03	20.26 ± 0.04	22.06 ± 0.08	20.05 ± 0.38
R 3	1	22:36:59.90	+34:28:00.7	385.4	544.3	24.67 ± 0.07	24.36 ± 0.19	24.74 ± 0.07	24.32 ± 0.97
R 4	1	22:36:59.69	+34:28:04.2	301.9	595.6	25.47 ± 0.09	22.36 ± 0.12	25.53 ± 0.06	22.38 ± 0.53
R 5	2	22:36:59.05	+34:28:31.7	356.0	190.0	24.42 ± 0.05	24.14 ± 0.17	24.47 ± 0.09	24.44 ± 0.37
R 6	2	22:36:56.71	+34:28:31.9	648.0	214.9	22.07 ± 0.02	19.82 ± 0.10	22.12 ± 0.10	19.85 ± 0.15
R 7	2	22:36:58.07	+34:28:56.4	457.9	448.6	23.45 ± 0.05	21.22 ± 0.12	23.45 ± 0.08	21.24 ± 0.05
R 8	2	22:36:57.52	+34:28:56.0	525.8	450.4	25.08 ± 0.05	23.58 ± 0.10	25.03 ± 0.10	23.50 ± 0.07
R 9	2	22:36:58.05	+34:28:58.9	458.1	473.5	20.54 ± 0.07	19.78 ± 0.11	20.60 ± 0.08	19.80 ± 0.07
R 10	2	22:36:57.94	+34:29:05.9	465.7	545.4	25.12 ± 0.07	24.93 ± 0.16	25.14 ± 0.07	24.85 ± 0.20
R 11	3	22:37:02.11	+34:28:27.4	121.6	117.1	25.47 ± 0.08	25.02 ± 0.23	25.51 ± 0.04	25.07 ± 0.19
R 12	3	22:37:01.90	+34:29:13.0	582.4	127.2	23.54 ± 0.06	22.76 ± 0.45	23.58 ± 0.04	22.95 ± 0.10
R 13	3	22:37:02.37	+34:29:13.5	583.3	185.9	24.67 ± 0.07	24.42 ± 0.15	24.78 ± 0.05	24.37 ± 0.10
R 14	3	22:37:02.48	+34:29:03.8	484.5	192.9	24.81 ± 0.07	23.83 ± 0.13	24.83 ± 0.04	23.76 ± 0.06
R 15	3	22:37:02.84	+34:28:22.6	64.2	204.1	25.11 ± 0.09	24.32 ± 0.10	25.23 ± 0.08	24.26 ± 0.04
R 16	3	22:37:03.06	+34:28:36.1	200.0	243.1	24.44 ± 0.06	23.95 ± 0.60	24.48 ± 0.04	24.31 ± 0.07
R 17	3	22:37:05.45	+34:28:51.0	326.9	552.6	24.31 ± 0.08	21.35 ± 0.16	24.30 ± 0.06	21.36 ± 0.08
R 18	3	22:37:05.57	+34:28:49.7	312.6	567.1	25.47 ± 0.07	22.77 ± 0.20	25.46 ± 0.05	22.88 ± 0.07
R 19	3	22:37:05.97	+34:29:15.4	567.3	637.6	23.68 ± 0.07	20.77 ± 0.14	23.82 ± 0.04	20.81 ± 0.05
R 20	3	22:37:06.12	+34:29:02.0	430.4	645.0	23.35 ± 0.06	21.03 ± 0.12	23.38 ± 0.03	21.04 ± 0.04
R 21	3	22:37:06.41	+34:28:50.3	310.0	672.1	25.32 ± 0.08	22.26 ± 0.13	25.35 ± 0.06	22.27 ± 0.05
R 22	3	22:37:06.45	+34:29:13.6	545.3	695.1	25.00 ± 0.08	22.33 ± 0.11	25.05 ± 0.03	22.30 ± 0.07
R 23	4	22:37:03.47	+34:28:11.4	271.2	128.6	24.98 ± 0.06	24.85 ± 0.14	24.97 ± 0.10	24.78 ± 0.12
R 24	4	22:37:02.85	+34:28:03.3	189.8	207.1	24.73 ± 0.06	24.51 ± 0.10	24.71 ± 0.07	24.37 ± 0.10
R 25	4	22:37:03.68	+34:27:59.6	288.5	248.4	25.04 ± 0.08	24.61 ± 0.06	25.00 ± 0.06	24.48 ± 0.12
R 26	4	22:37:04.11	+34:27:50.9	339.3	343.2	21.28 ± 0.09	19.72 ± 0.12	21.22 ± 0.03	19.70 ± 0.07
R 27	4	22:37:05.62	+34:27:50.7	526.8	358.9	24.64 ± 0.06	24.28 ± 0.14	24.51 ± 0.07	24.09 ± 0.06
R 28	4	22:37:05.09	+34:27:48.6	459.0	374.7	24.63 ± 0.06	24.18 ± 0.26	24.60 ± 0.06	24.14 ± 0.17
R 29	4	22:37:05.59	+34:27:40.4	515.9	462.1	24.66 ± 0.07	24.01 ± 0.55	24.64 ± 0.06	24.25 ± 0.08
R 30	4	22:37:05.21	+34:27:33.8	463.8	525.6	24.06 ± 0.06	23.62 ± 0.59	24.02 ± 0.04	23.84 ± 0.13
R 31	4	22:37:03.26	+34:27:23.1	213.0	616.7	24.11 ± 0.07	23.26 ± 0.13	24.01 ± 0.07	23.13 ± 0.14

Table 3. ALLFRAME – DoPHOT Comparison.

Chip	N	ΔV	ΔI
1	4	-0.143 ± 0.061	$+0.110 \pm 0.068$
2	6	-0.022 ± 0.019	-0.035 ± 0.062
3	12	-0.050 ± 0.015	-0.047 ± 0.037
4	9	$+0.050 \pm 0.014$	$+0.029 \pm 0.052$

Table 4. Calibrated DoPHOT F555W_{0.5} and F814W_{0.5} magnitudes of Cepheids with good light curves.

Epoch	Single epoch magnitudes				
	V 1	V 2	V 3	V 4	V 5
F555W _{0.5} 1	26.00 ± 0.16	25.77 ± 0.13	27.20 ± 0.24	25.36 ± 0.12	25.93 ± 0.14
2	24.91 ± 0.12	26.44 ± 0.15	27.08 ± 0.23	26.20 ± 0.15	26.60 ± 0.20
3	25.43 ± 0.13	25.90 ± 0.13	26.48 ± 0.16	25.57 ± 0.12	26.08 ± 0.15
4	25.27 ± 0.13	26.15 ± 0.14	26.52 ± 0.15	25.71 ± 0.14	25.25 ± 0.13
5	25.56 ± 0.16	26.55 ± 0.18	27.37 ± 0.32	26.05 ± 0.16	25.62 ± 0.13
6	25.77 ± 0.14	26.26 ± 0.14	27.32 ± 0.26	26.29 ± 0.17	25.79 ± 0.14
7	26.19 ± 0.25	25.72 ± 0.14	26.67 ± 0.21	26.61 ± 0.24	26.37 ± 0.23
8	26.29 ± 0.14	25.51 ± 0.16	26.71 ± 0.21	26.86 ± 0.20	26.33 ± 0.17
9	25.10 ± 0.12	26.61 ± 0.18	26.44 ± 0.20	26.20 ± 0.14	26.25 ± 0.15
10	25.05 ± 0.11	26.18 ± 0.17	26.69 ± 0.19	26.16 ± 0.15	26.41 ± 0.16
11	25.45 ± 0.12	25.31 ± 0.13	27.32 ± 0.28	26.58 ± 0.18	25.59 ± 0.13
12	25.44 ± 0.17	25.94 ± 0.15	27.39 ± 0.29	25.90 ± 0.13	25.46 ± 0.12
13	26.14 ± 0.17	25.54 ± 0.14	27.50 ± 0.35	26.77 ± 0.19	26.24 ± 0.16
14	25.49 ± 0.15	25.11 ± 0.12	26.74 ± 0.23	26.81 ± 0.18	25.66 ± 0.14
15	26.28 ± 0.19	25.50 ± 0.13	26.36 ± 0.16	26.54 ± 0.19	...
F814W _{0.5} 1	24.92 ± 0.16	25.17 ± 0.16	26.33 ± 0.28	24.85 ± 0.13	24.67 ± 0.13
2	24.43 ± 0.15	25.66 ± 0.18	25.75 ± 0.20	25.34 ± 0.18	24.97 ± 0.14
9	24.08 ± 0.13	25.26 ± 0.17	26.20 ± 0.34	24.71 ± 0.13	25.03 ± 0.19
12	24.73 ± 0.21	24.84 ± 0.14	26.51 ± 0.41	24.80 ± 0.13	24.39 ± 0.12

Table 4—Continued

Epoch	Single epoch magnitudes				
	V 6	V 7	V 8	V 9	V 10
F555W _{0.5} 1	25.95 ± 0.16	25.68 ± 0.09	27.93 ± 0.46	25.93 ± 0.10	26.75 ± 0.21
2	26.57 ± 0.20	25.84 ± 0.11	27.21 ± 0.22	26.52 ± 0.19	26.59 ± 0.21
3	25.35 ± 0.14	26.09 ± 0.12	28.21 ± 0.37	26.60 ± 0.17	26.11 ± 0.17
4	25.49 ± 0.15	26.16 ± 0.13	28.18 ± 0.50	26.03 ± 0.10	26.67 ± 0.20
5	25.76 ± 0.16	26.15 ± 0.13	27.24 ± 0.26	26.03 ± 0.11	27.22 ± 0.26
6	25.68 ± 0.13	26.12 ± 0.13	26.89 ± 0.18	26.26 ± 0.12	27.15 ± 0.28
7	26.65 ± 0.26	25.61 ± 0.10	28.60 ± 1.13	26.49 ± 0.19	26.74 ± 0.23
8	26.66 ± 0.20	25.58 ± 0.08	27.33 ± 0.24	27.05 ± 0.29	27.95 ± 0.48
9	25.31 ± 0.15	25.91 ± 0.12	26.93 ± 0.21	26.13 ± 0.11	27.59 ± 0.40
10	25.43 ± 0.15	25.89 ± 0.11	26.48 ± 0.14	26.19 ± 0.14	27.56 ± 0.44
11	25.58 ± 0.15	26.40 ± 0.17	28.41 ± 0.66	26.58 ± 0.16	27.46 ± 0.35
12	26.32 ± 0.20	25.71 ± 0.10	26.81 ± 0.20	25.91 ± 0.11	27.43 ± 0.41
13	25.94 ± 0.18	26.39 ± 0.15	28.28 ± 0.57	26.55 ± 0.18	26.74 ± 0.23
14	...	25.51 ± 0.08	27.30 ± 0.23	26.58 ± 0.17	27.43 ± 0.37
15	26.53 ± 0.18	26.06 ± 0.12	27.69 ± 0.41	26.45 ± 0.17	28.23 ± 0.62
F814W _{0.5} 1	25.29 ± 0.21	24.49 ± 0.08	26.70 ± 0.41	24.71 ± 0.10	25.70 ± 0.23
2	25.15 ± 0.17	24.77 ± 0.09	26.06 ± 0.22	25.07 ± 0.12	25.45 ± 0.23
9	25.50 ± 0.26	24.56 ± 0.14	26.37 ± 0.42	24.88 ± 0.12	25.98 ± 0.36
12	25.29 ± 0.21	24.56 ± 0.09	25.68 ± 0.18	24.62 ± 0.09	26.80 ± 0.63

Table 4—Continued

Epoch	Single epoch magnitudes		
	V 11	V 12	V 13
F555W _{0.5} 1	25.71 ± 0.15	26.29 ± 0.20	25.93 ± 0.16
2	26.40 ± 0.18	25.39 ± 0.14	26.66 ± 0.26
3	26.02 ± 0.18	25.91 ± 0.17	25.36 ± 0.13
4	26.01 ± 0.17	25.94 ± 0.18	25.40 ± 0.13
5	26.25 ± 0.18	26.08 ± 0.20	25.53 ± 0.13
6	26.42 ± 0.29	25.56 ± 0.16	25.96 ± 0.16
7	26.40 ± 0.23	25.39 ± 0.15	25.90 ± 0.21
8	26.05 ± 0.15	25.51 ± 0.14	26.10 ± 0.17
9	26.87 ± 0.26	26.15 ± 0.21	26.41 ± 0.21
10	26.55 ± 0.22	26.09 ± 0.22	26.28 ± 0.22
11	25.79 ± 0.14	25.31 ± 0.13	25.60 ± 0.13
12	26.29 ± 0.17	25.79 ± 0.17	25.86 ± 0.14
13	25.89 ± 0.15	25.55 ± 0.16	26.08 ± 0.20
14	25.81 ± 0.14	26.12 ± 0.22	25.51 ± 0.14
15	26.20 ± 0.23	25.86 ± 0.25	26.60 ± 0.21
F814W _{0.5} 1	24.96 ± 0.17	25.10 ± 0.18	24.98 ± 0.20
2	25.48 ± 0.23	24.41 ± 0.14	25.06 ± 0.17
9	25.15 ± 0.21	24.94 ± 0.20	25.08 ± 0.23
12	25.18 ± 0.20	24.75 ± 0.17	24.68 ± 0.17

Table 5. Calibrated ALLFRAME F555W_{0.5} and F814W_{0.5} magnitudes of Cepheids with good light curves.

Epoch	Single epoch magnitudes				
	V 1	V 2	V 3	V 4	V 5
F555W _{0.5} 1	26.09 ± 0.26	25.66 ± 0.13	27.30 ± 0.28	25.65 ± 0.19	25.97 ± 0.14
2	24.97 ± 0.11	26.11 ± 0.18	26.70 ± 0.23	26.19 ± 0.13	26.39 ± 0.17
3	25.42 ± 0.12	...	26.63 ± 0.20	25.52 ± 0.13	26.20 ± 0.21
4	...	25.81 ± 0.16	26.63 ± 0.23	25.66 ± 0.13	25.52 ± 0.17
5	...	26.41 ± 0.25	27.23 ± 0.35	26.05 ± 0.16	25.76 ± 0.11
6	25.49 ± 0.90	26.13 ± 0.21	27.42 ± 0.30	26.28 ± 0.16	26.04 ± 0.19
7	25.90 ± 0.33	25.62 ± 0.19	26.52 ± 0.20	26.39 ± 0.31	26.17 ± 0.25
8	26.05 ± 0.18	25.38 ± 0.16	26.78 ± 0.21	27.00 ± 0.25	26.25 ± 0.17
9	25.01 ± 0.10	26.21 ± 0.19	...	26.16 ± 0.21	26.32 ± 0.14
10	25.05 ± 0.13	25.96 ± 0.47	26.66 ± 0.22	26.22 ± 0.17	26.52 ± 0.19
11	25.29 ± 0.13	25.15 ± 0.20	27.32 ± 0.27	26.54 ± 0.18	25.70 ± 0.13
12	25.31 ± 0.13	25.91 ± 0.11	27.86 ± 0.43	25.99 ± 0.15	25.57 ± 0.13
13	26.17 ± 0.15	25.47 ± 0.12	27.67 ± 0.49	27.03 ± 0.22	26.48 ± 0.16
14	25.05 ± 0.12	25.22 ± 0.13	26.76 ± 0.20	26.85 ± 0.32	25.67 ± 0.21
15	26.16 ± 0.18	25.69 ± 0.16	26.48 ± 0.15	26.49 ± 0.26	27.01 ± 0.29
F814W _{0.5} 1	24.86 ± 0.14	25.08 ± 0.14	26.22 ± 0.23	24.86 ± 0.12	24.67 ± 0.07
2	24.20 ± 0.09	25.45 ± 0.16	25.71 ± 0.19	25.20 ± 0.10	25.02 ± 0.11
8	24.06 ± 0.13	25.16 ± 0.24	26.33 ± 0.39	24.78 ± 0.13	25.39 ± 0.23
12	24.33 ± 0.15	25.08 ± 0.12	26.67 ± 0.36	25.04 ± 0.13	24.81 ± 0.11

Table 5—Continued

Epoch	Single epoch magnitudes				
	V 6	V 7	V 8	V 9	V 10
F555W _{0.5}	25.55 ± 0.14	25.62 ± 0.12	28.02 ± 0.58	25.89 ± 0.13	27.00 ± 0.31
2	25.97 ± 0.24	26.00 ± 0.19	27.40 ± 0.37	26.57 ± 0.38	26.79 ± 0.32
3	25.05 ± 0.11	26.26 ± 0.18	27.53 ± 0.44	25.89 ± 0.22	26.60 ± 0.34
4	25.07 ± 0.12	26.16 ± 0.16	28.38 ± 0.74	26.05 ± 0.12	26.75 ± 0.27
5	25.42 ± 0.13	26.15 ± 0.13	27.43 ± 0.37	26.06 ± 0.16	27.36 ± 0.45
6	25.54 ± 0.14	26.10 ± 0.15	27.01 ± 0.24	26.38 ± 0.18	27.27 ± 0.34
7	26.03 ± 0.24	25.56 ± 0.19	...	26.44 ± 0.26	26.70 ± 0.26
8	25.96 ± 0.33	25.71 ± 0.11	27.40 ± 0.34	27.03 ± 0.35	27.61 ± 0.40
9	24.92 ± 0.11	25.88 ± 0.17	26.51 ± 1.13	25.98 ± 0.15	27.68 ± 0.51
10	25.02 ± 0.11	26.00 ± 0.10	26.64 ± 0.22	26.25 ± 0.22	27.68 ± 0.51
11	25.40 ± 0.14	26.28 ± 0.24	28.18 ± 0.59	26.52 ± 0.19	27.21 ± 0.34
12	26.36 ± 0.23	25.70 ± 0.14	26.92 ± 0.23	25.82 ± 0.14	27.53 ± 0.36
13	25.61 ± 0.16	26.43 ± 0.22	27.83 ± 0.77	26.45 ± 0.19	26.90 ± 0.22
14	24.97 ± 0.11	25.61 ± 0.13	27.60 ± 0.30	26.48 ± 0.23	27.43 ± 0.38
15	26.45 ± 0.21	26.12 ± 0.17	27.77 ± 0.50	26.60 ± 0.26	28.26 ± 0.86
F814W _{0.5} 1	24.58 ± 0.10	24.65 ± 0.16	26.83 ± 0.44	24.84 ± 0.16	25.75 ± 0.19
2	24.94 ± 0.13	24.87 ± 0.16	26.20 ± 0.34	25.10 ± 0.13	25.66 ± 0.22
8	25.19 ± 0.22	24.74 ± 0.17	26.76 ± 0.44	25.06 ± 0.21	26.09 ± 0.33
12	25.16 ± 0.13	24.76 ± 0.15	25.97 ± 0.25	24.73 ± 0.12	26.91 ± 0.72

Table 5—Continued

Epoch	Single epoch magnitudes		
	V 11	V 12	V 13
F555W _{0.5} 1	25.95 ± 0.20	26.29 ± 0.25	26.23 ± 0.32
2	26.65 ± 0.22	25.32 ± 0.10	26.78 ± 0.25
3	26.20 ± 0.33	25.96 ± 0.18	25.39 ± 0.14
4	26.10 ± 0.16	25.94 ± 0.16	25.44 ± 0.20
5	26.26 ± 0.24	25.95 ± 0.17	25.58 ± 0.13
6	26.64 ± 0.24	25.53 ± 0.15	25.83 ± 0.14
7	26.69 ± 0.38	25.36 ± 0.16	25.99 ± 0.33
8	25.88 ± 0.19	25.56 ± 0.23	26.22 ± 0.17
9	26.97 ± 0.41	26.03 ± 0.22	26.51 ± 0.17
10	26.80 ± 0.25	26.11 ± 0.26	26.47 ± 0.17
11	25.81 ± 0.15	25.16 ± 0.15	25.61 ± 0.16
12	26.50 ± 0.23	26.07 ± 0.30	26.08 ± 0.19
13	26.24 ± 0.20	25.53 ± 0.17	26.42 ± 0.25
14	25.90 ± 0.13	26.26 ± 0.19	25.67 ± 0.15
15	26.46 ± 0.23	26.23 ± 0.22	26.58 ± 0.31
F814W _{0.5} 1	25.17 ± 0.15	25.36 ± 0.17	25.20 ± 0.17
2	25.67 ± 0.29	24.59 ± 0.10	25.20 ± 0.14
8	25.39 ± 0.22	25.02 ± 0.20	25.01 ± 0.24
12	25.55 ± 0.24	24.98 ± 0.14	24.91 ± 0.15

Table 6. Parameters for Cepheids Detected in NGC 7331.

ID	Chip	RA (J2000)	Dec	X	Y	P_{Alf}	$\langle V \rangle_{Alf}$	$\langle V - I \rangle_{Alf}$	P_{Doph}	$\langle V \rangle_{Doph}$	$\langle V - I \rangle_{Doph}$
V 1	2	22:36:59.61	+34:28:20.1	296.3	75.1	42.59	25.40 ± 0.06	1.08 ± 0.09	42.18	25.53 ± 0.04	0.89 ± 0.09
V 2	2	22:36:56.52	+34:28:42.2	661.8	322.1	21.19	25.68 ± 0.06	0.50 ± 0.10	21.35	25.81 ± 0.04	0.54 ± 0.09
V 3	2	22:36:58.30	+34:28:45.9	437.8	340.7	13.91	26.93 ± 0.08	0.95 ± 0.16	13.91	26.91 ± 0.06	0.94 ± 0.17
V 4	2	22:36:58.82	+34:28:47.4	372.4	350.4	22.60	26.13 ± 0.05	1.20 ± 0.08	22.60	26.14 ± 0.04	1.12 ± 0.08
V 5	2	22:37:00.23	+34:29:26.7	162.1	732.2	33.94	26.16 ± 0.05	1.10 ± 0.08	33.87	26.02 ± 0.04	1.30 ± 0.09
V 6	2	22:36:59.92	+34:29:28.2	199.8	750.4	29.05	25.62 ± 0.05	0.91 ± 0.08	29.43	26.02 ± 0.06	0.81 ± 0.12
V 7	3	22:37:01.81	+34:28:41.3	265.1	88.9	39.90	25.89 ± 0.04	1.08 ± 0.09	39.72	25.86 ± 0.03	1.22 ± 0.06
V 8	3	22:37:02.74	+34:28:51.7	360.3	212.1	11.13	27.37 ± 0.13	0.97 ± 0.23	11.16	27.47 ± 0.12	1.40 ± 0.20
V 9	3	22:37:03.13	+34:28:57.1	410.6	265.2	24.41	26.20 ± 0.06	1.27 ± 0.10	25.83	26.37 ± 0.04	1.52 ± 0.07
V 10	4	22:37:03.41	+34:28:07.9	261.1	163.3	11.61	27.02 ± 0.11	1.05 ± 0.25	11.61	26.96 ± 0.09	1.04 ± 0.22
V 11	4	22:37:04.53	+34:27:27.8	371.8	575.5	19.82	26.28 ± 0.06	0.93 ± 0.14	19.86	26.15 ± 0.05	0.98 ± 0.11
V 12	4	22:37:04.53	+34:27:25.6	369.7	597.4	24.82	25.68 ± 0.05	0.86 ± 0.09	26.68	25.65 ± 0.05	0.99 ± 0.10
V 13	4	22:37:03.80	+34:27:06.9	266.6	779.3	41.20	25.92 ± 0.05	1.27 ± 0.10	37.54	25.92 ± 0.05	1.16 ± 0.11

Table 7. Fits to PL relations.

Sample	N	DM(V)	DM(I)	$E(V - I)^a$	DM $_0^a$
ALLFRAME					
All	13	31.36 ± 0.07	31.17 ± 0.04	0.19 ± 0.06	30.89 ± 0.08
P > 15	10	31.32 ± 0.07	31.15 ± 0.04	0.17 ± 0.07	30.90 ± 0.08
P > 20	9	31.33 ± 0.07	31.15 ± 0.04	0.18 ± 0.08	30.90 ± 0.08
P > 25	5	31.52 ± 0.08	31.31 ± 0.05	0.21 ± 0.05	31.01 ± 0.09
DoPHOT					
All	13	31.41 ± 0.08	31.16 ± 0.06	0.25 ± 0.07	30.80 ± 0.14
P > 15	10	31.38 ± 0.10	31.18 ± 0.07	0.21 ± 0.09	30.88 ± 0.16
P > 20	9	31.41 ± 0.10	31.20 ± 0.08	0.21 ± 0.10	30.90 ± 0.18
P > 25	7	31.50 ± 0.10	31.24 ± 0.09	0.26 ± 0.10	30.86 ± 0.20

Note. — (a) Due to the finite width of the Cepheid instability strip, errors in DM(V) and DM(I) are partially correlated when calculating the errors in $E(V - I)$ and DM $_0$.

Table 8. Error Budget.

Source of Uncertainty	Error (mag)	Notes
CEPHEID PL CALIBRATION		
(a) LMC True Modulus	± 0.10	(1)
(b) V PL Zero Point	± 0.05	(2),(3)
(c) I PL Zero Point	± 0.03	(2),(4)
(S1) Systematic Uncertainty	± 0.12	(a),(b),(c) combined in quadrature
NGC 7331 MODULUS		
(d) HST V-Band Zero Point	± 0.04	(5)
(e) HST I-Band Zero Point	± 0.04	(5)
(R1) Cepheid True Modulus	± 0.11	(6)
(f) PL Fit (V) (ALLFRAME)	± 0.07	(7)
(g) PL Fit (I) (ALLFRAME)	± 0.04	(7)
(R2) Cepheid True Modulus	± 0.08	(f),(g) partially correlated, (8)
(S2) Metallicity Uncertainty	$+0.05 \pm 0.04$	See text for details
TOTAL UNCERTAINTY		
(R) Random Errors	± 0.14	(R1) and (R2) combined in quadrature
(S) Systematic Errors	$+0.05 \pm 0.13$	(S1) and (S2) combined in quadrature

Note. — (1) Adopted from Westerlund (1997).

(2) Derived from the observed scatter in the Madore & Freedman (1991) PL relation, with 32 contributing LMC Cepheids.

(3) V-band scatter: ± 0.27 .

(4) I-band scatter: ± 0.18 .

(5) Contributing uncertainties from aperture corrections, the Holtzman et al. (1995) zero points, and the long-versus short uncertainty, combined in quadrature. Adopted aperture correction contribution is the worst case formal uncertainty (± 0.02 mag) for the NGC 7331 aperture corrections. Adopted Holtzman et al. (1995) zero point uncertainty is ± 0.02 mag. Adopted long-versus-short-exposure correction uncertainty is ± 0.02 mag.

(6) Assuming that photometric errors (d,e) are uncorrelated between filters, and noting that the V and I magnitudes are multiplied by +1.45 and -2.45, respectively, when correcting for reddening, results in a derived error on the true modulus of $[(1.45)^2(0.04)^2 + (-2.45)^2(0.04)^2]^{1/2} = 0.11$ mag.

(7) Uncertainties for the mean apparent V and I moduli are limited by the apparent width of the derived PL relation, reduced by the population size of contributing Cepheids for NGC 7331 (13 variables). Contributing effects include photometric errors, differential reddening and intrinsic strip filling. (8) The partially correlated nature of the derived PL width uncertainties is taken into account by the (correlated) dereddening procedure, coupled with the largely “degenerate-with-reddening” positioning of individual Cepheids within the instability strip.

Table 9. Comparison of Published Distances to NGC 7331.

Method	Distance (Mpc)	Reference
Sizes of HII regions	9.1	Sersic 1960
Luminosity Class	7.9	van den Bergh 1960
$H_0 = 75$	14.4	Rubin et al. 1965
M31/NGC 7331 diameters	15.4	Rubin et al. 1965
Mass estimators	13.0	Balkowski et al. 1973
Tully-Fisher (H band)	10.1	Aaronson et al. 1980, 1982a
Velocity ratio with Virgo	12.0	Aaronson et al. 1982a
Sizes of dark clouds	7.2	Osman et al. 1982
Tully-Fisher (B band)	9.6	Bottinelli et al. 1985
$H_0 = 75$	14.3	Tully 1988
Cepheids	15.1	This paper (ALLFRAME)

Table 10. IRTF Calibration.

Galaxy	DM	$\log\Delta V$	H_g^{abs}	Source of Distance
NGC 224 (M31)	24.40	2.751	-23.93	Freedman & Madore 1990
NGC 300	26.66	2.371	-19.99	Madore & Freedman 1991
NGC 598 (M33)	24.50	2.392	-20.50	Freedman 1990
NGC 925	29.84	2.422	-21.48	Silbermann et al. 1996
NGC 2090	30.45	2.529	-21.98	Phelps et al. 1998
NGC 2403	27.50	2.488	-21.29	Freedman 1990
NGC 3031 (M81)	27.80	2.716	-23.62	Freedman et al. 1994
NGC 3351 (M95)	30.01	2.573	-22.72	Graham et al. 1997
NGC 3368 (M96)	30.32	2.709	-23.60	Tanvir et al. 1995
NGC 3621	29.13	2.536	-22.43	Rawson et al. 1997
NGC 4536	31.10	2.576	-22.99	Saha et al. 1996
NGC 7331	30.89	2.740	-24.81	This paper

Note. — ΔV are the 21 cm line widths in km/s, as listed in Table 4 of Tormen & Burstein (1995), which are from Aaronson et al (1982a), and corrected for inclination and z , but without any 3° addition term to the inclinations. H_g mags are from Tormen & Burstein (1995), which are the Aaronson et al. (1982a) $H_{0.5}$ mags recalculated in accordance with the isophotal diameters of RC3, and uncorrected for inclination.

Table 11. NGC 7331 Group.

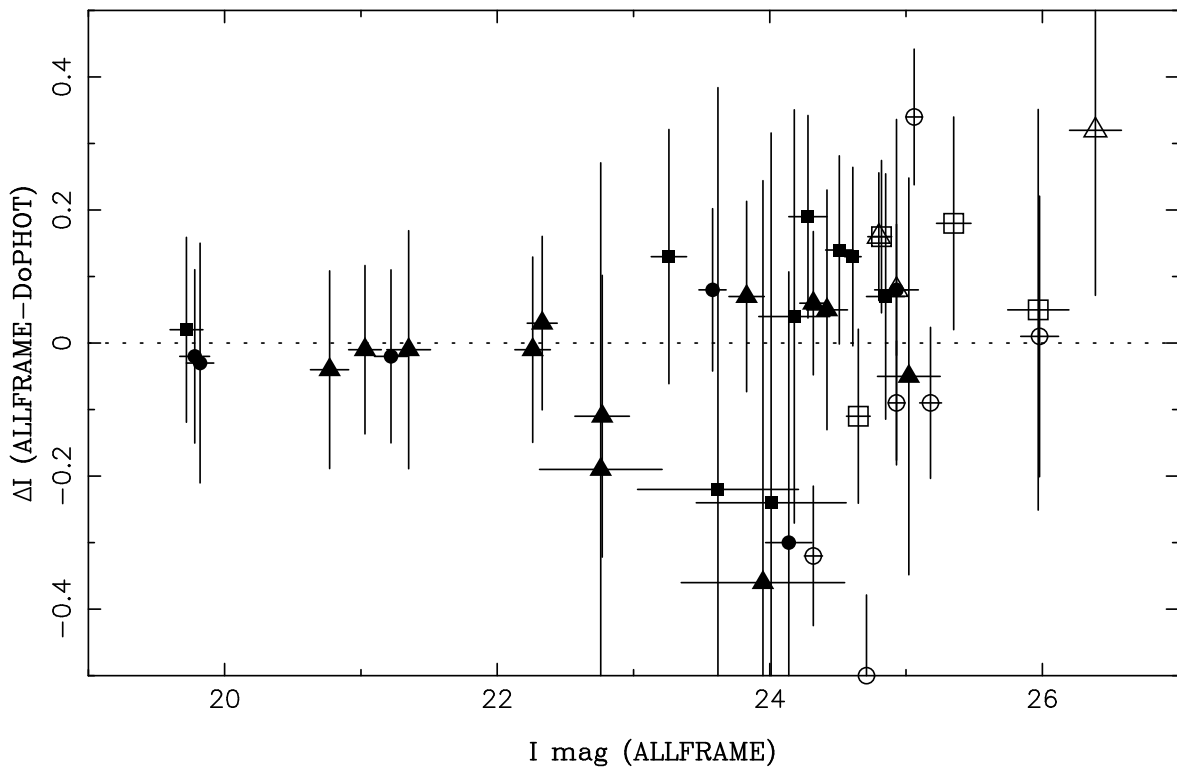
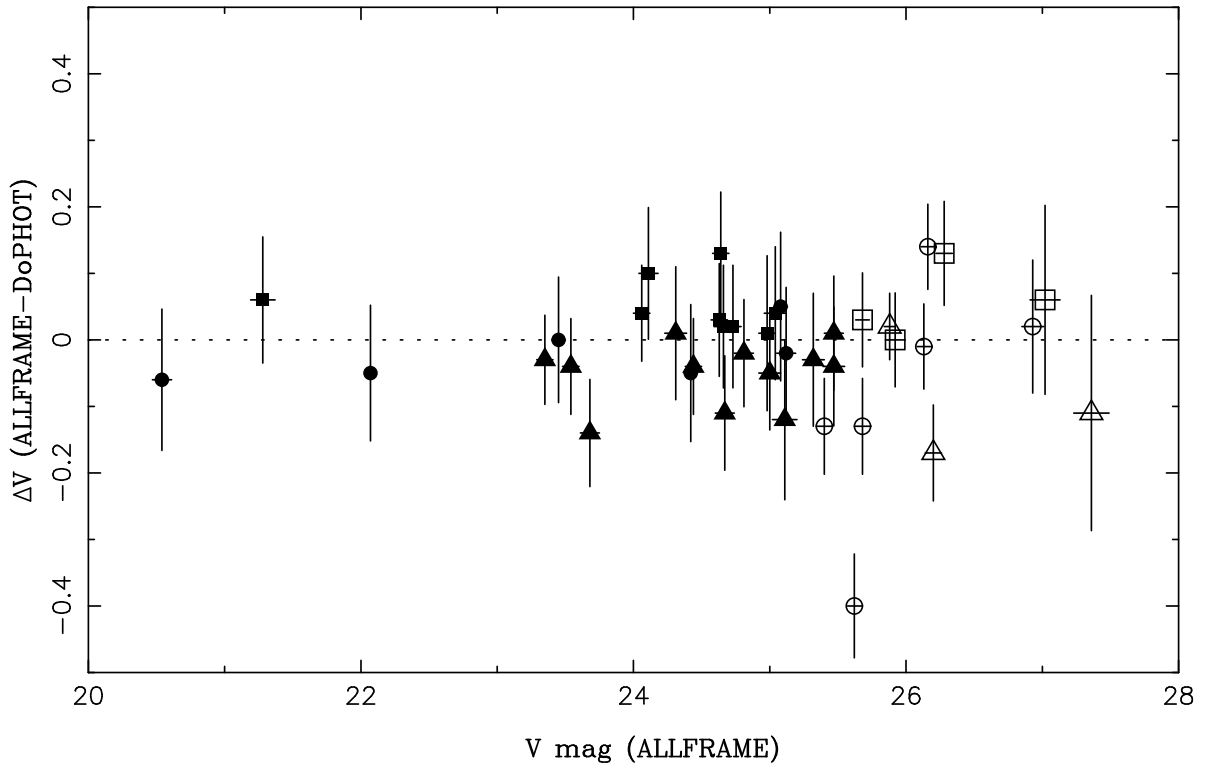
Galaxy	RA (J2000)	Dec	V_{hel} km s $^{-1}$	R (degrees)
NGC 7217	22:07:52.1	+31:21:35	1195	6.85
NGC 7292	22:28:25.0	+30:17:30	1226	4.50
2228+3300	22:29:36.8	+33:17:17	1130	1.92
UGC 12060	22:30:33.9	+33:49:11	1128	1.47
UGC 12082	22:34:10.9	+32:51:31	1047	1.66
NGC 7320A	22:36:03.4	+33:56:54	1029	0.51
NGC 7331	22:37:04.0	+34:24:57	1064	0.00
UGC 12212	22:50:29.5	+29:08:15	1120	6.00
NGC 7457	23:00:59.8	+30:08:39	1054	6.63
UGC 12311	23:01:23.8	+30:14:08	1150	6.62
UGC 12404	23:11:04.8	+29:38:39	1066	8.64

Table A1. DoPHOT Aperture Correction Spatial Coefficients.

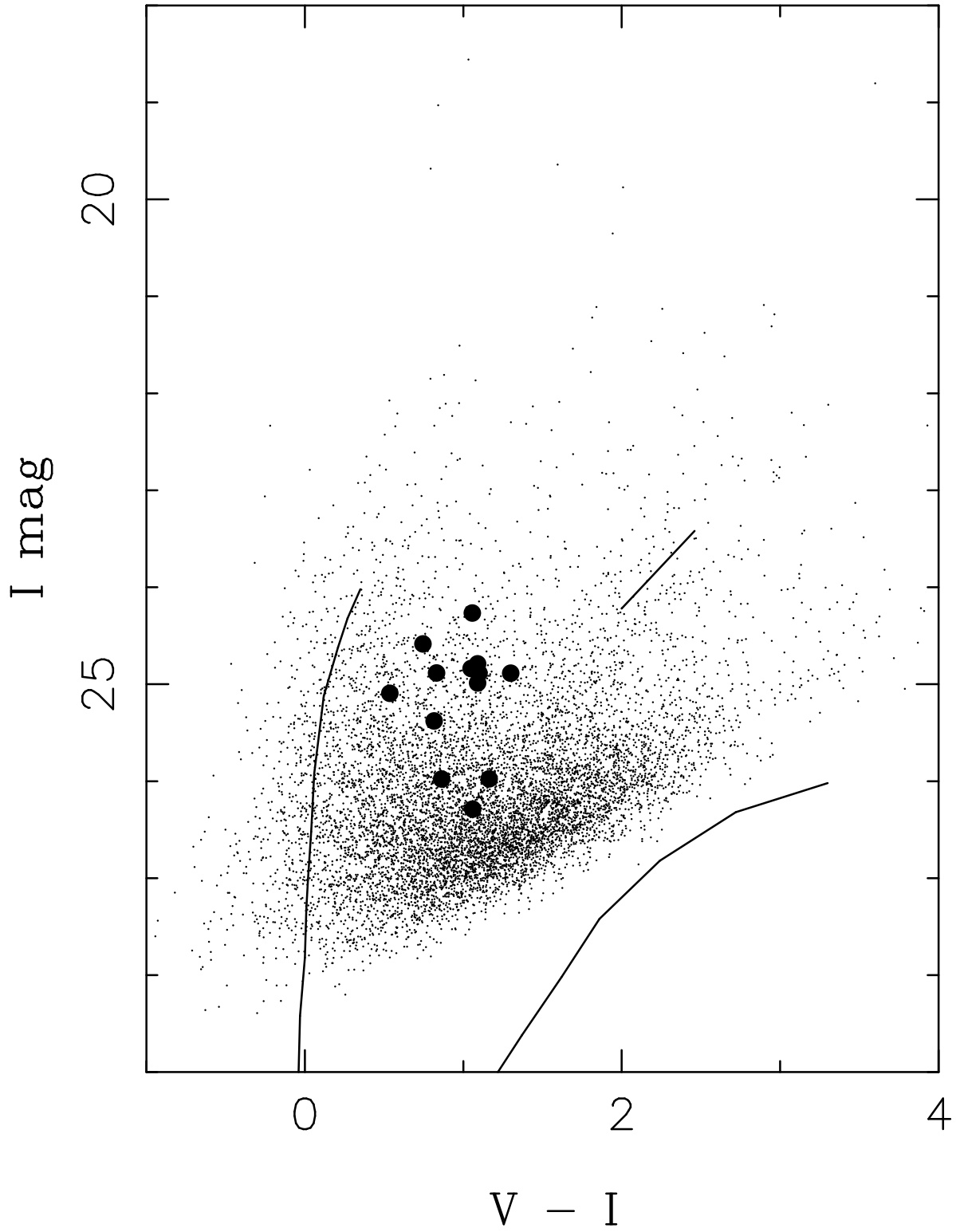
Chip	C0	C1	C2	C3	C4	C5
F555W						
1	−0.99431	7.222919E-5	3.826290E-4	−7.732423E-8	−4.587308E-7	−7.685230E-9
2	−0.817943	1.941904E-4	3.665115E-4	−3.065632E-7	−4.345170E-7	1.143239E-7
3	−0.73354	2.550644E-5	3.484296E-4	−7.614571E-8	−4.447892E-7	1.363507E-7
4	−0.818136	2.384645E-4	4.255572E-4	−3.253283E-7	−6.087260E-7	7.968657E-8
F814W						
1	0.550125	7.906689E-5	1.449731E-4	−2.173195E-7	−2.504804E-7	2.752383E-7
2	−0.914758	1.835472E-4	2.947996E-4	−2.878237E-7	−3.648580E-7	1.434279E-7
3	−0.884129	7.124484E-6	2.373478E-4	−1.044799E-7	−3.485253E-7	2.285843E-7
4	−0.949892	2.751133E-4	3.490840E-4	−2.675065E-7	−3.724136E-7	−1.041973E-7

Table A2. Zero-points and Aperture Corrections.

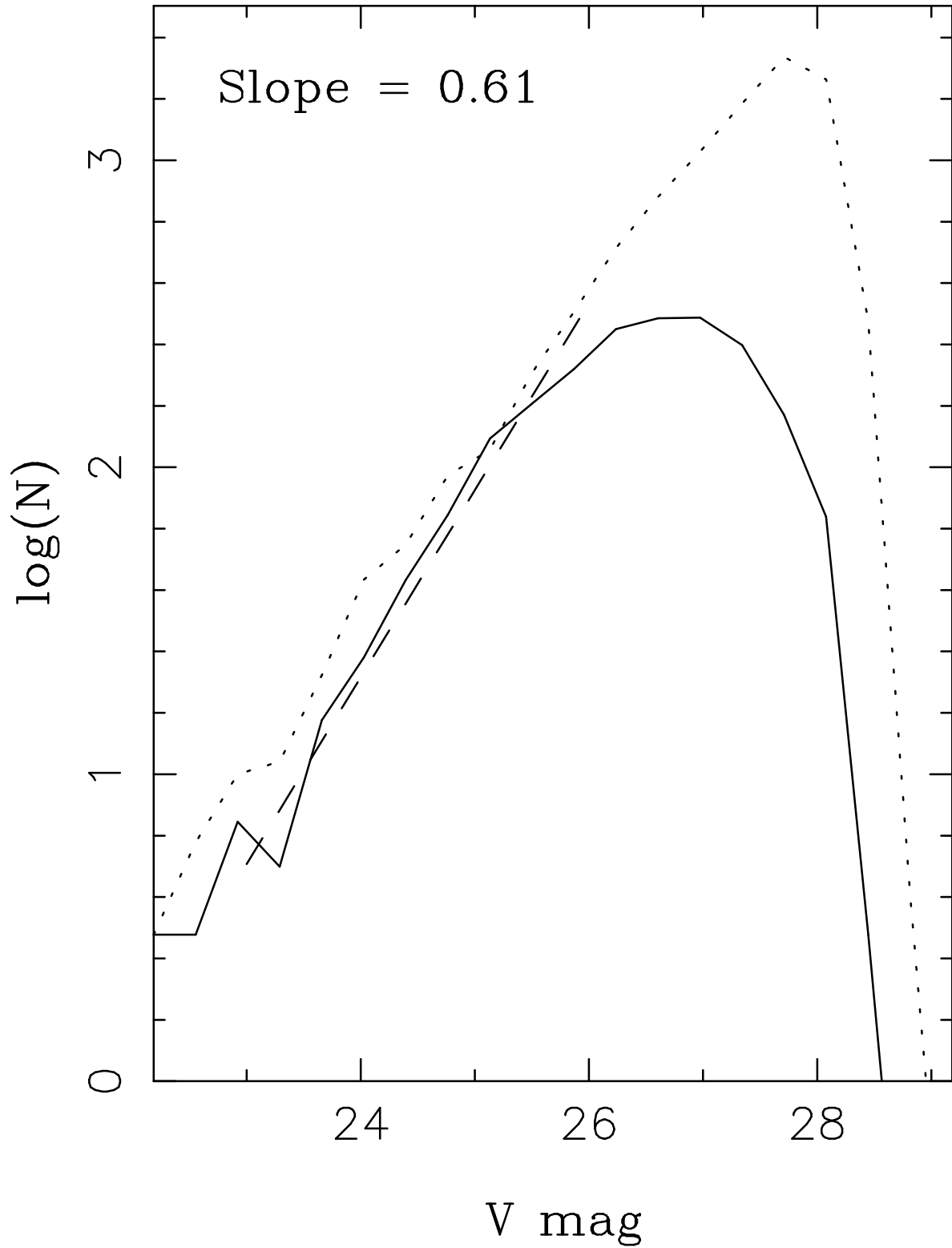
Filter	Chip PC1	Chip WF2	Chip WF3	Chip WF4
DoPHOT Zero-points				
F555W	−7.630	−7.536	−7.554	−7.559
F814W	−8.536	−8.381	−8.436	−8.441
ALLFRAME Mean Aperture Corrections				
F555W	−0.062	+0.031	+0.029	+0.058
F814W	−0.051	+0.069	+0.036	+0.070
ALLFRAME Zero-points				
F555W	−0.967	−0.958	−0.950	−0.973
F814W	−1.861	−1.823	−1.842	−1.870

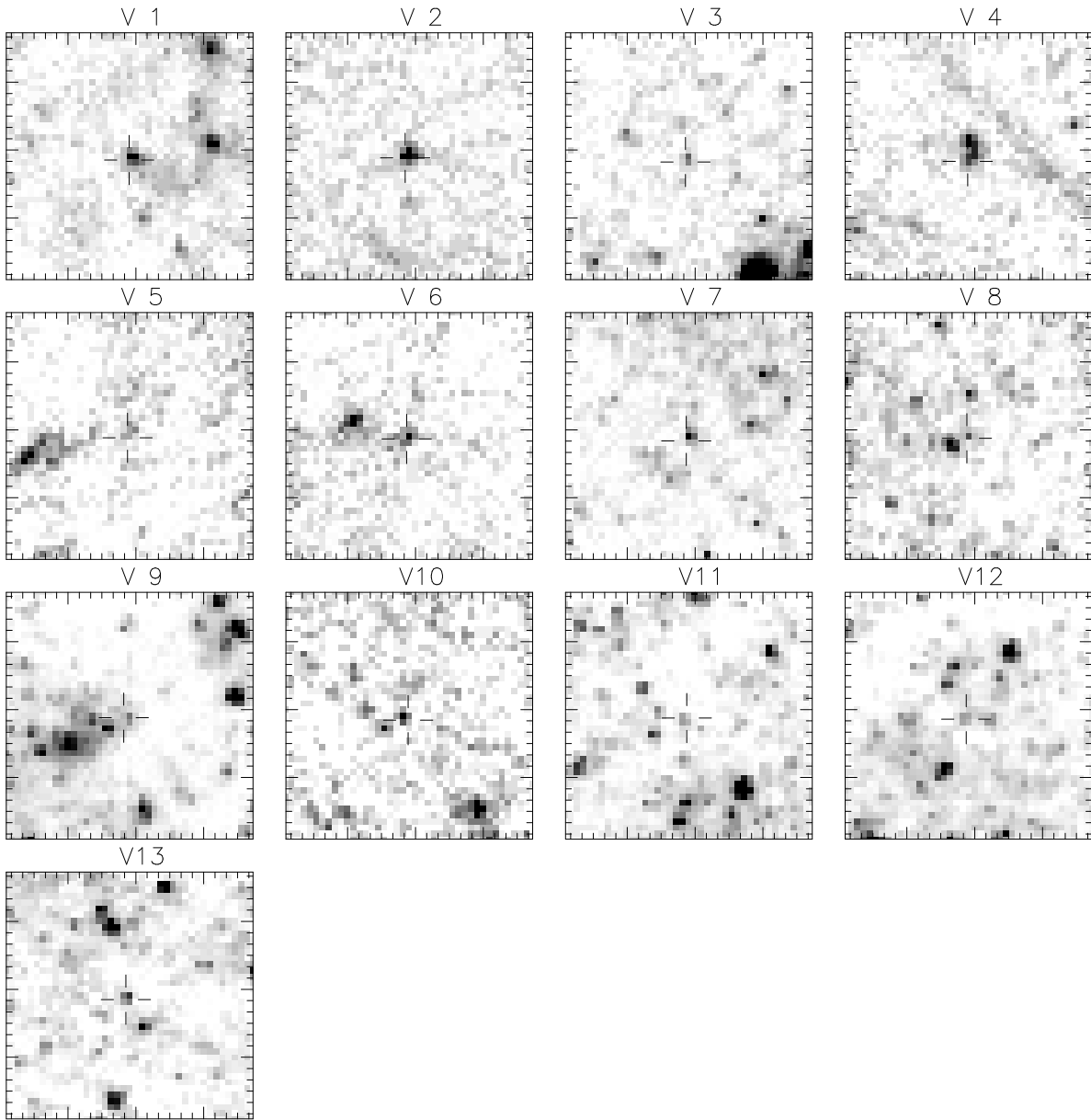


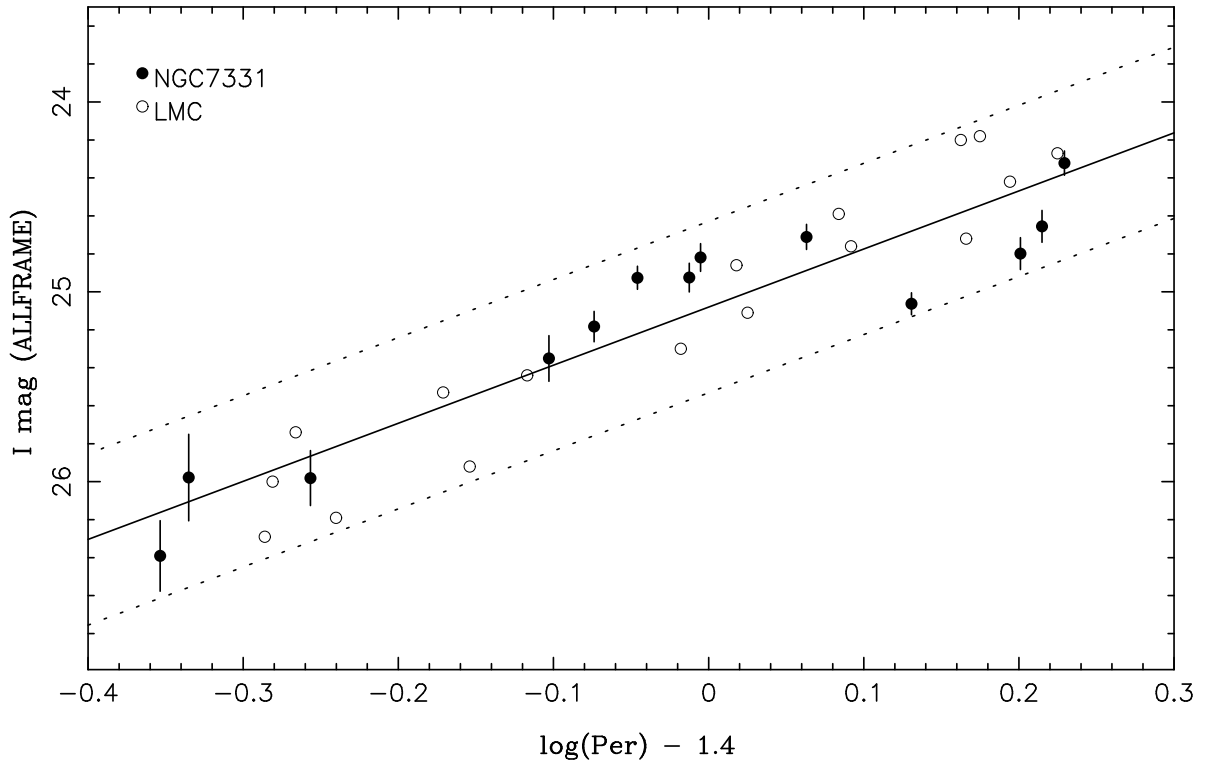
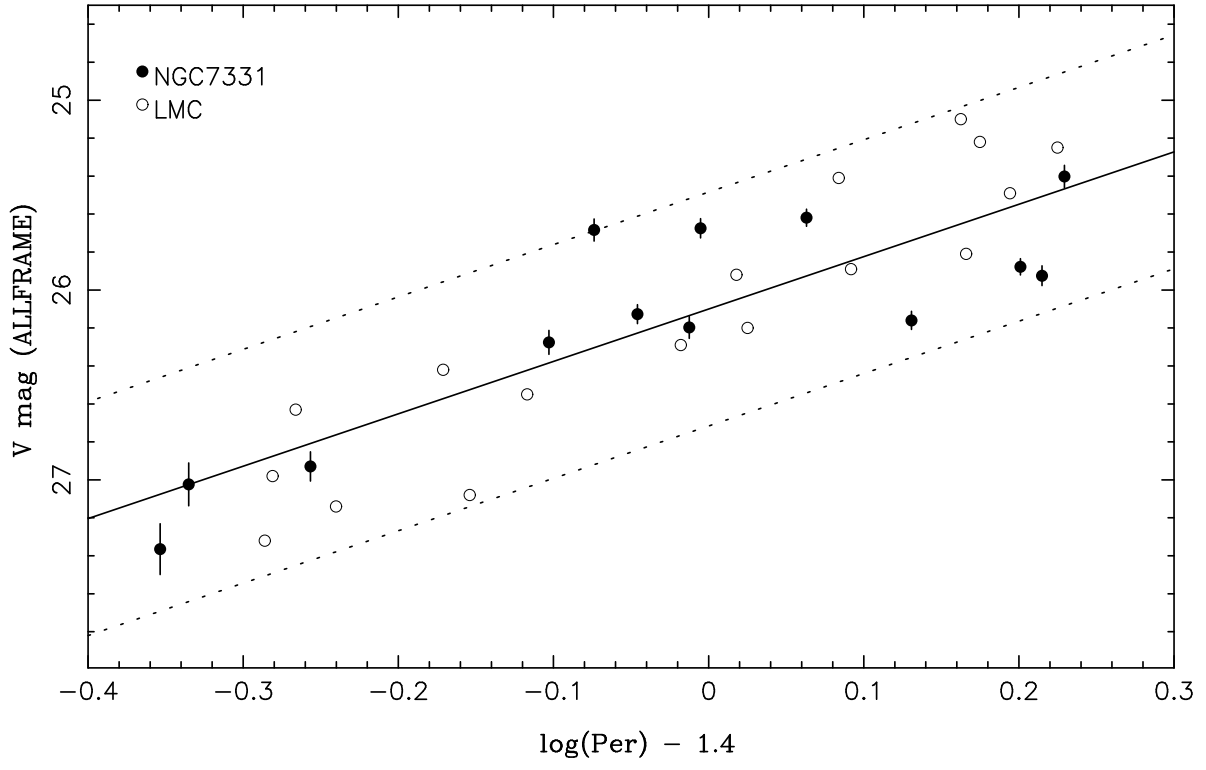
NGC 7331

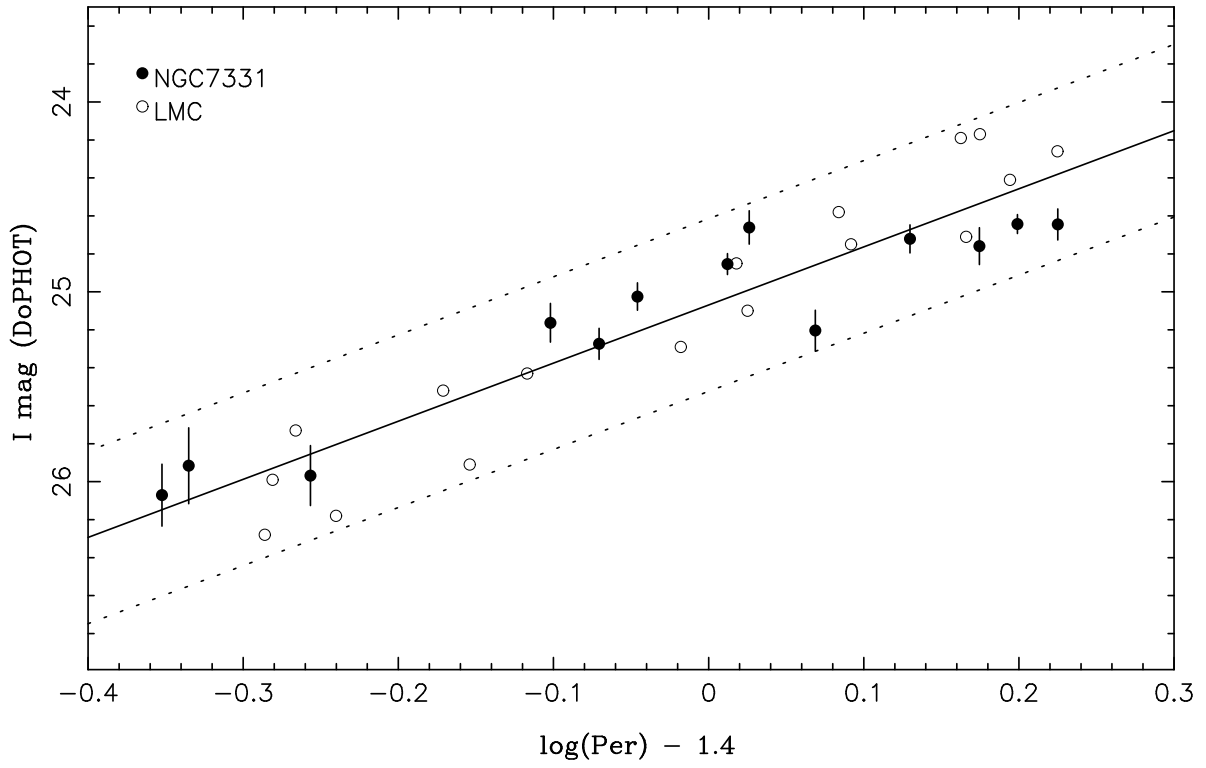
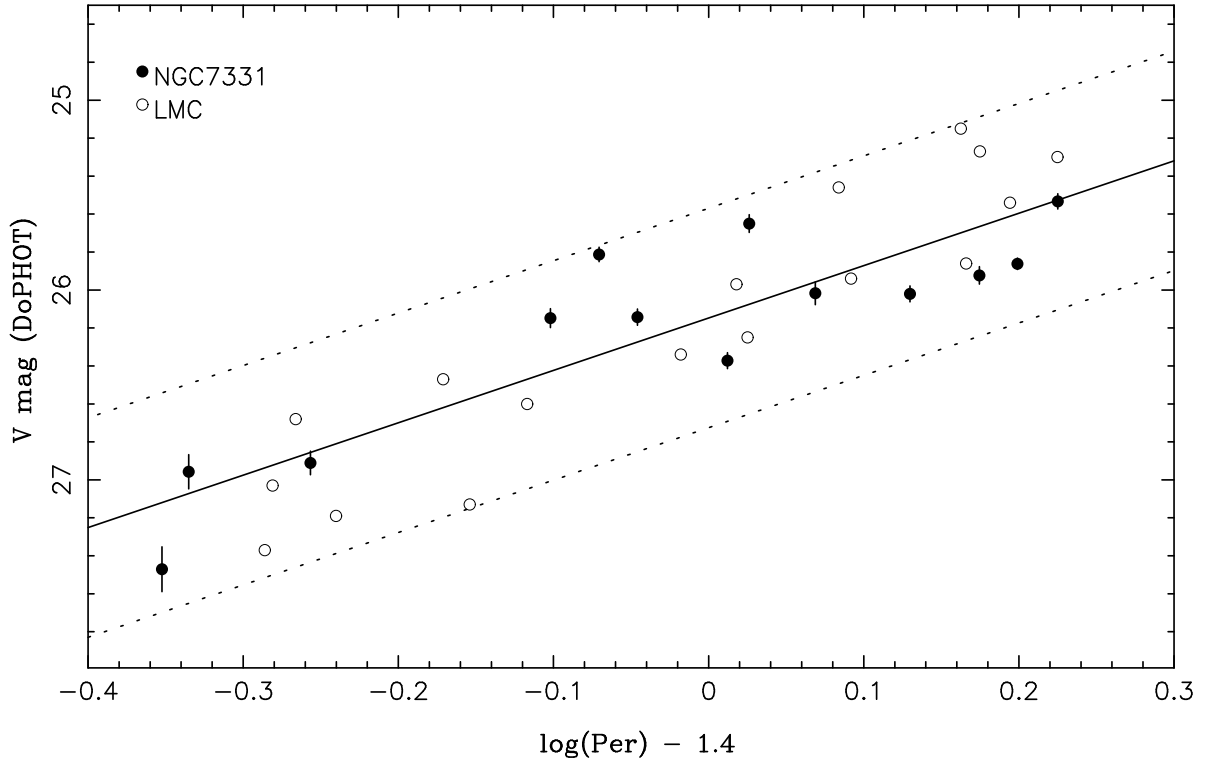


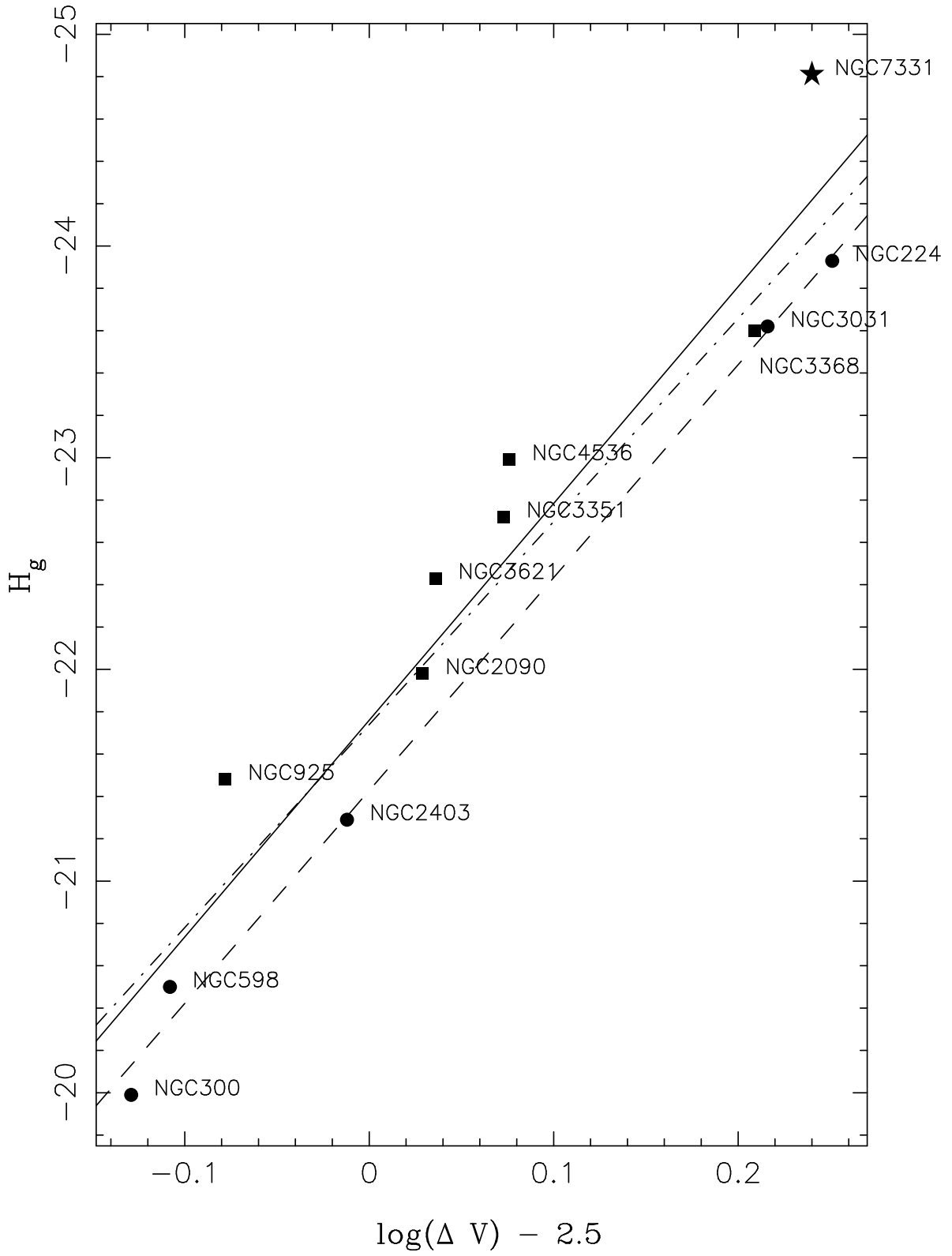
NGC 7331











This figure "n7331_f01.jpg" is available in "jpg" format from:

<http://arxiv.org/ps/astro-ph/9802184v1>

This figure "n7331_f02.jpg" is available in "jpg" format from:

<http://arxiv.org/ps/astro-ph/9802184v1>